Enzyme Assisted Nanolithography

Leif Riemenschneider

Doctoral Dissertation
University of Bremen
Department of Biophysics

Abstract

In this work a method is developed to chemically immobilize proteins on the apex of the tip of an atomic force microscope (AFM) in order to chemically or physically modify surfaces with high spatial resolution.

The feasibility of this method is demonstrated exemplarily with the enzyme alkaline phosphatase and the substrate 5-bromo-4-chloro-indoxyl-phosphate (BCIP) and the cofactor nitro-blue-tetrazol (NBT). The product of the enzymatic reaction precipitates and it is possible to deposit it locally by bringing the functionalized tip in the vicinity of a suitable surface.

The deposition of single spots and continuous contours with typical dimensions of 10 nm in height and 150-170 nm laterally is demonstrated. Estimation of the number of immobilized enzymes on the apex of the AFM tip suggest a number of approximately 40 enzymes. This novel method was dubbed *Enzyme-assisted Nanolithography*. The universality of this technique gives it a "tool box" character, which allows the employment of many different proteins.

The second part of this work deals with the attempt to regulate the activity of immobilized enzymes by adjusting the pH value in their vicinity by the application of electric surface potentials. So far it was not possible to demonstrate the feasibility of this concept. A theoretical analysis will be given and suggestions for improved experiments are made.

The third part describes the development of a self-built AFM. The instrument features small physical dimensions which make it suitable for fast imaging of samples. The software is based entirely on Open Source components, thus allowing easy modification and adaption of the instrument to new requirements.

Acknowledgments

First of all I would like to thank Manfred Radmacher and Monika Fritz for providing me with the opportunity to work in their group. I especially appreciate the freedom I was given in approaching and solving the problems that were encountered and also for the support I received regarding my family. Special thanks to Monika for answering all those "physicist questions" to me when it came to chemistry.

I want to thank Sven Blank for teaching me the basics, for valuable discussions throughout this work and for good company in general. Marcus Prass, thanks for asking those good questions that made me think and for the clean fun. Arne Schäfer, thank you for the entertainment. The world would be a boring but quiet place without you. Laura Treccani, Andrea Moldovan and Meike Gummich I want to thank for their company and especially for those yummy cakes. Thank you Christina Kenst, Edda Thoma and Ilona Bär for your help in ordering, telling me where to find stuff and for standing the mess in the lab that I sometimes left.

Holger Doschke and Hartmut Rohbeck I want to thank for their help on the technical side and for providing the good connection to the workshop. Hermann Neuhaus and Detlef Lambrecht from the mechanical workshop have my appreciation for the skillful construction of the mechanical AFM parts. Denise Loske, thank you for the straight forward help with the electron beam evaporation. Ulrike Schulz and Kerstin von Rhode have my appreciation for their support and company in Göttingen.

Finally, I want to thank my parents, who have constantly encouraged and supported me, and express my deepest love to Henna: thanks for giving me the opportunity of deepening my studies and for everything else.

Bremen, June 2004

Leif R.

Contents

Part I

Enzyme Assisted Nanolithography

I

Introduction

The most exciting phrase to hear in science,
the one that heralds new discoveries,
is not "Eureka!" (I found it) but
"That's funny..."

Isaac Asimov

1.1 Introduction

For many decades, lithographic processes have been commonplace in the semiconductor industry, where structures with feature sizes of hundredth of nanometers are routinely produced. Although these photo-lithographic methods are extremely high developed and potential for decreasing the feature size still exists (UV lithography), its limitations are foreseeable. Owing to obstacles such as leakage currents and limited heat dissipation of devices that are produced by classical photo-lithographic methods, the search for fundamentally different approaches to computing has become a field of intense research. Prominent examples of attempts to develop new techniques are for example CPUs or memories that are based on carbon nanotubes [1], polymers [2] or DNA [3].

Not only the need for computers and memories drives this research but also the desire to design and miniaturize biological assays like DNA and protein chips or biosensors for diagnostic devices.

Clearly, new methods demand new tools. Because the majority of these new functional units are created or located on surfaces, a variety of methods have been developed that allow their modification. A widely used approach is for example the *micro contact printing*, in which a pattern of some substance is transferred from the channels of an elastomeric stamp onto a solid substrate [4]. Another technique that has attracted a lot of interest is the so called *dip pen lithography* [5], in which an AFM tip is coated with

an appropriate “ink”, which then is deposited onto a surface. The resolution of both methods is in the order of a hundred nanometer but the techniques allow only the *deposition* of material. A method that would additionally allow the chemical and physical modification with high spatial resolution would be a valuable tool in the design of new experiments and applications.

Chemical reactions in the context of biological systems are often mediated by proteins. Especially proteins with catalytic properties, so called enzymes, are of technological interest.

Enzymes have been used to chemically modify surfaces locally by applying them with a micro pipette to a sample that had been coated with a substrate of the enzyme [6]. The feature size of the produced structures was in the order of a few 10 micrometer.

Obtaining higher spatial resolution and avoiding the release of the enzymes into the bulk of the solution would be a favorable improvement for such an experiment.

An instrument that provides outstanding spatial control, when it comes to positioning a probe, is the atomic force microscope (AFM). Utilizing this unique instrument for the physical and chemical modification of surfaces potentially opens the door for many exiting experiments.

This work attempts to combine the high spatial resolution of an AFM with the ability of enzymes to modify a substrate not only physically but also chemically. Ultimately these modifications should be possible at the single molecule level.

2

Atomic Force Microscopy

Nobody is bored when he is trying
to make something that is beautiful,
or to discover something that is true.

William Inge

2.1 Basics

The *Atomic Force Microscope* (AFM) was originally developed in 1986 by Binnig et al. [7] at the IBM San Jose Research Labs. It allows to obtain various types of information of surfaces, by utilizing a very sharp tip that is moved over a sample in a raster fashion. This tip has usually a pyramidal shape and is protruding from the end of a cantilever. The radius of curvature of the apex is typically 15 nm (Fig. 2.1).

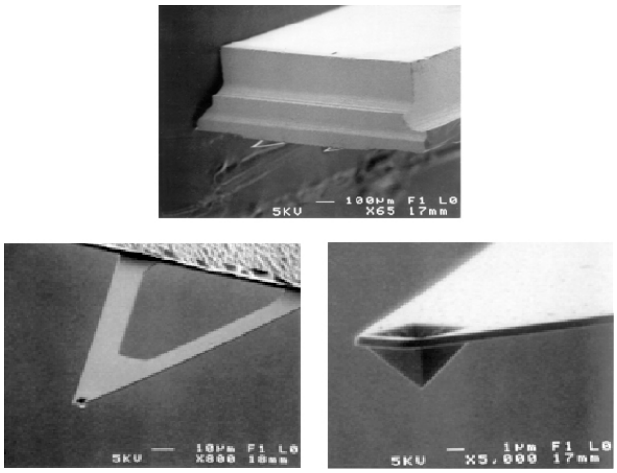

Figure 2.1. Electron microscope images of a commercial AFM cantilever – Successive magnification of the pyramidal tip [8].

Due to the interaction between the tip and the surface the cantilever gets deflected and twisted while it scans over the surface. By measuring these two attributes, information about the topography and the local friction can be obtained. The material of choice for an AFM cantilever is often silicon-nitride because of its hardness and its production compatibility with lithographic processes used in the semiconductor industry.

One feature, that makes the AFM exceedingly well suited for the study of biological specimens is the possibility to have the AFM tip submerged in a fluid. In the case of proteins or living cells a buffer solution can provide conditions in which they are stable and functional. This ability makes the AFM an unique instrument that allows to study biological samples under native conditions with high spatial resolution.

2.2 Working Principle

Information, such as the topography or the friction of a sample, is obtained from the deflection and torsion of the cantilever while it scans over the surface. The movement of the cantilever is detected with the help of a laser beam that is focused on the reflective backside of the cantilever (Fig. 2.2). The reflected beam then illuminates a photodiode that is subdivided into four parts (quadrant-diode). Prior to an experiment the laser beam is adjusted so that the same amount of intensity falls onto each quadrant. Once the cantilever gets deflected due to the interaction with the sample, the reflected beam path will change, which results in a vertical shift of the laser spot position on the quadrant-diode. By measuring the light intensity on each quadrant and by summing up the corresponding voltages as $V_{def} = (A + B) - (C + D)$ the resulting V_{def} is proportional to the physical deflection of the cantilever.

To minimize the force on the sample, the measured deflection is used to calculate the value for a vertical displacement of the sample relative to the tip, in order to maintain a constant deflection. This is done by means of an active feedback loop which continously adjusts the vertical position of the sample according to the measured deflection. Generally, the movement in all directions (X,Y,Z) is achieved by using a piezoelectric translation unit.

2.3 Modes of Operation

An AFM can be operated in two distinct modes:

- Contact Mode:
  In contact mode the cantilever gets deflected mainly due to the hard-core repulsion of the atomic orbitals of the sample and the tip. The deflection is directly measured by the afore mentioned method. The advantage of this mode is the high spatial resolution and the relatively high speed at which the sample can be scanned. The disadvantage is the relatively high force that is laterally exerted on the sample.

- Tapping Mode:
  In this mode the cantilever oscillates with a certain frequency and amplitude. This oscillation is driven by a piezo that is attached close to the chip mounting (Fig. 2.2). The information about the interaction between tip and sample is contained in the amplitude of the oscillation, which is extracted from the regular deflection signal and is then processed in the feedback loop. The advantage of this setup is that already before tip and sample undergo repulsive interaction, long-range attractive interactions (Van der Waals, electrostatics) attenuate the amplitude of the oscillation. Therefore the lateral and vertical forces that act on the sample are smaller than in contact mode, which makes it feasible to study more delicate samples. Disadvantages compared to the contact mode are the lower spatial resolution and the slower scanning speed caused by the requirement to determine the amplitude of the oscillation.
  This mode of operation was developed in 1994 by Putman [9] and Hansma [10].

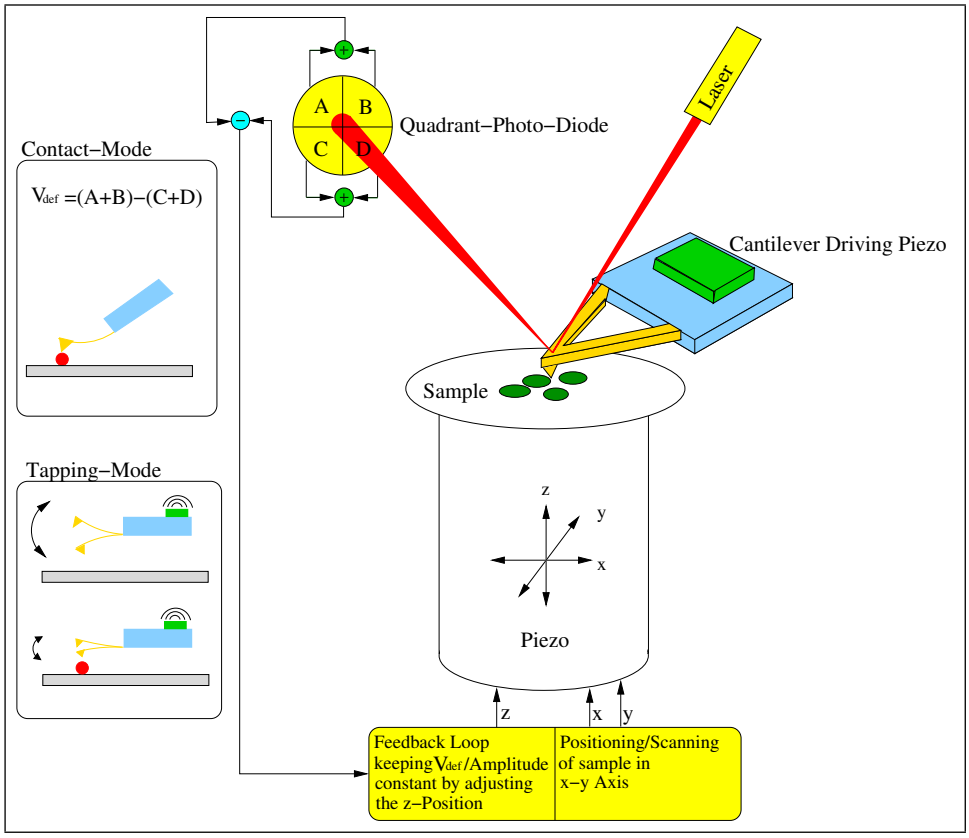

Figure 2.2. Schematics of an AFM – Illustration of Contact Mode and Tapping Mode

3

Proteins

There can be no twisted thought
without a twisted molecule.

R. W. Gerard

3.1 Proteins

Most biochemical processes in living organisms are mediated by proteins. Proteins are macromolecules that consist of chains of aminoacids, which are linked by peptide bonds. Most organisms have 20 different aminoacids at their disposal for the synthesis of proteins.

The aminoacid chain usually folds into compact arrangements, whose function and structure depends on the distinctive sequence of the aminoacids.

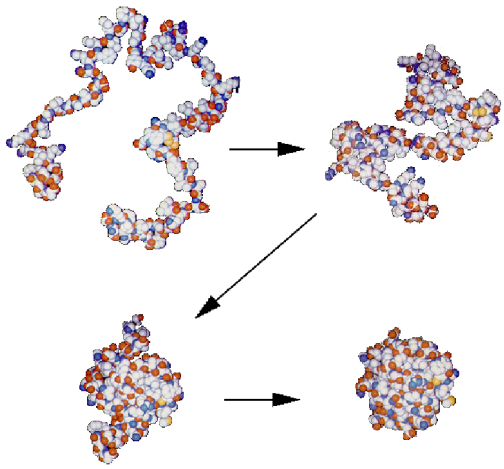

Figure 3.1. Illustration for the folding of a aminoacid chain into a functional protein. Based on [11].

Proteins fulfill an enormous amount of different tasks, of which some important functions in living organisms are:

- Catalysis of chemical reactions
  - Often these proteins show a very high specificity to a certain substrate. An illustrative example is the protein α-*Amylase*, which hydrolyzes saccharide bonds, thus breaking down the saccharide polymer starch into its monomeric subunits. Proteins that show catalytic behavior are called *Enzymes*.
- Structural elements
  - Important proteins of the cytoskeleton are for example *Actin*, which polymerizes into long thin fibers or α-*Tubulin* and β-*Tubulin* which make up the so called microtubuli.
- Antibodies
  - As part of the immune-defense these Y-shaped proteins exhibit two binding sites which allows them to bind specifically to certain antigens.
- Hormones
  - Prominent examples of proteins that have a hormonal function are *Insulin* and *Erythropoietin* better known as EPO. EPO is notorious for its abuse in competitive sports as a doping substance by promoting the proliferation of red blood cells.
- Electron carriers
  - The most famous representative in this group is *Cytochrome-c* which is a protein that functions as an electron carrier in photosynthesis.

In the context of this work we are interested in *enzymes* with their ability to promote distinct chemical reactions.

3.2 Alkaline Phosphatase

The protein employed in this work is a representative of a class of proteins called *Alkaline Phosphatase* (AP). In almost all living organisms this protein is present and it is performing the task of catalyzing the hydrolysis of organic phosphomonoesters [12].

$$\mathbf{R-O-PO_3H_2 + H_2O \longrightarrow R-OH + HO-PO_3H_2} \tag{3.1}$$

In this reaction scheme the R-group can stand for different components, of which polysaccharides, polynucleotides or glycerides are common representatives in cells. The AP used in this study is isolated from bovine calf intestine and consists of two almost identical subunits with a total molecular weight of 160 kDa. Since the best studied representative of these proteins comes from the bacterium Escherichia Coli and because its structure is known from xray-diffraction to a resolution of 2Å [13], it will be used as a proxy for the graphical representations of the AP used in this work. Figure 3.2 shows the structure of AP from E. Coli. with a closeup of the active site [14]. For the structural stability and the catalytic activity of AP the bivalent ions Mg^{++} and Zn^{++} need to be present at the active site [15]. The shape can be described as an ellipsoid with a length of 5 nm and a width of 8 nm.

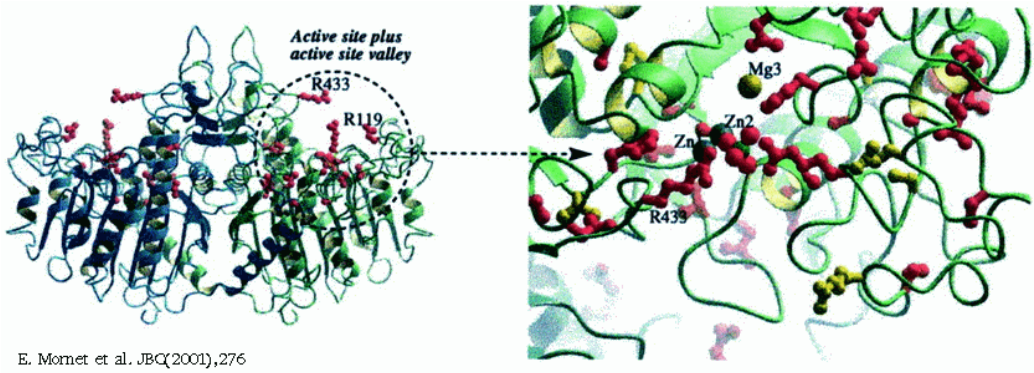

Figure 3.2. Ribbon model of E. Coli. AP with a closeup of the active site which shows the Mg and Zn ions required for the structural stability and the catalytic activity [14].

3.3 Streptavidin

Streptavidin is a tetrameric protein, in which each monomer exhibits a beta-barrel fold and has a molecular weight of approximately 16 kDa (Fig. 3.3). What makes streptavidin a remarkable protein is the fact that it binds non-covalently with an extraordinary high affinity to a ligand called *biotin* (Fig. 3.4). The dissociation constant is in the order of 10^{-15} M [16] and the streptavidin-biotin complex is stable over wide pH and temperature range. The origin of the strong interaction are hydrophobic and van der Waals interactions, an effective hydrogen bonding network and a binding surface loop,

which folds over the ligand [17]. Since each monomeric subunit has one biotin binding site, the entire tetrameric complex allows the binding of four ligands. Moreover it is easily possible to conjugate streptavidin and biotin with other proteins or molecules, thus providing means of immobilizing or selecting them for further processing.
All these properties make streptavidin a very attractive molecule to be used in many biotechnological applications.

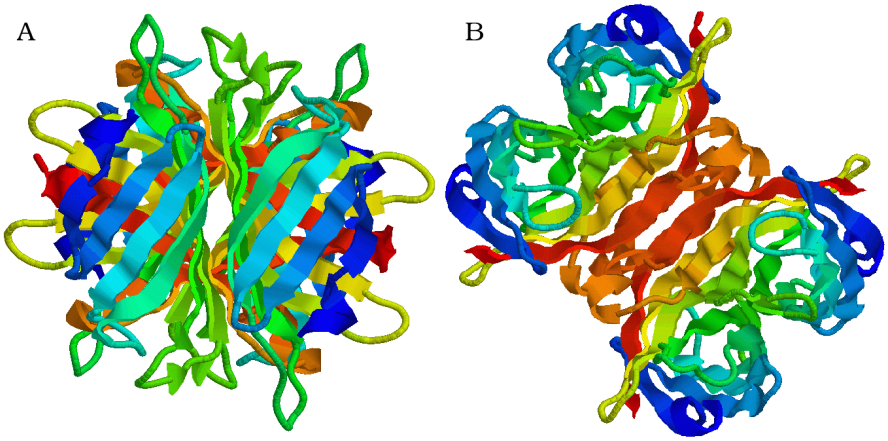

Figure 3.3. Side (A) and top (B) view of streptavidin, based on a generic molecular structure from the RCSB database [18].

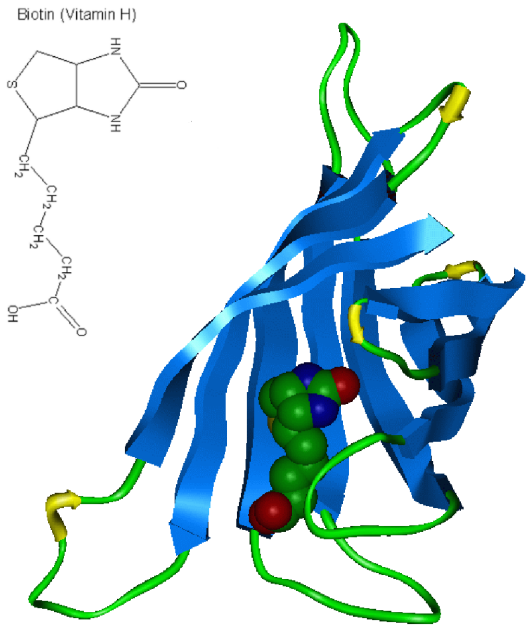

Figure 3.4. Depiction of a monomeric streptavidin subunit with a biotin ligand in the binding pocket. The strong non-covalent binding originates from hydrophobic and van der Waals interactions, an effective hydrogen bonding network and a binding surface loop, which folds over the ligand.

4

Immobilization of Proteins

We all admire the wisdom of people
who come to us for advice.

Jack Herbert

4.1 Introduction

The need to immobilize proteins on surfaces arises in many biotechnological applications, such as biosensors or bioseperators. Therefore, a variety of methods have been developed for different materials like SiO_2 (glass) [19], gold [20] or polymers [21].

Generally, the immobilization is realized by linker molecules that display binding sites on each end for either the protein or the support. The support is usually functionalized before being exposed to the protein that is to be immobilized. Often this surface modification is carried out in many steps, in which the functional surface is build up in a layer fashion. In the case of SiO_2 the surface is often functionalized in a first step with a *silane* molecule. This group of linear molecules is characterized by having a functional group on one end, which can form covalent bonds with the silanol groups of a substrate surface, and a great variety of other functional groups on the other end. This other functional group can for example be an *epoxy* group, which reacts efficiently with the primary amine groups of proteins (Fig. 4.1) [22].

Attempts to use this method resulted in non-functional proteins, because they were bound too tightly to the surface. The reason is that the AP displays primary amines all over its exterior. Such a tight binding can result in partial unfolding as well as steric hindrance of conformational changes that are associated with the protein activity.

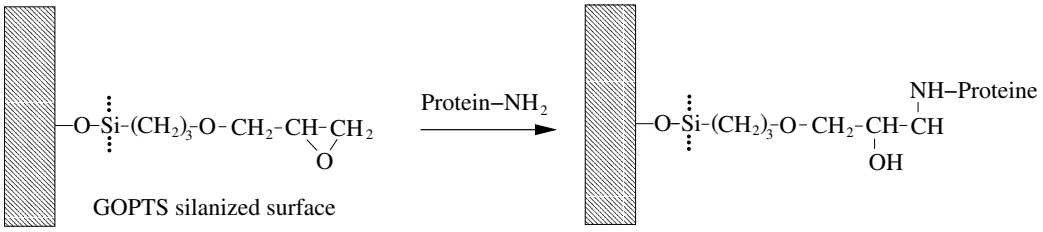

Figure 4.1. Immobilization of proteins via their primary amines. The epoxy-group of 3-glycidoxy-propyl-trimethoxy-silane (GOPTS) binds to the amine-groups of a protein. In the case of alkaline phosphatase this approach results in non-functional proteins.

4.2 Streptavidin-Biotin Immobilization

Because of the lack of success to attach the proteins via direct binding of the primary amines with GOPTS, it was necessary to resort to a different immobilization scheme. As lined out in section 3.3, the protein streptavidin and the ligand biotin undergo a very strong non-covalent binding. Since it is possible to conjugate streptavidin with other proteins, without interfering with their function, these complexes can be immobilized on a surface that has been functionalized with biotin groups.

Because alkaline phosphatase is commercially available as a streptavidin-conjugate, it was only necessary to biotinylate the surface on which the protein was supposed to be immobilized. In the case of SiO_2 a procedure was deployed that is depicted in Figure 4.2.

In a first step the cleaned surface was exposed to *N-2-aminoethyl-3-amino-propyl-trimethoxy-silane* (EDA) which forms a self assembled monolayer (SAM) on the surface, leaving it amine-functionalized. In a second step the sample was immersed in a solution of biotin-N-hydroxysuccinimide-ester (NHS-biotin), which binds to the primary amines. This surface was then ready to bind streptavidin-conjugated components via the displayed biotin sites. The distance between surface and the biotin size is approximately 3 nm. A detailed protocol of the preparation is presented in Appendix B.

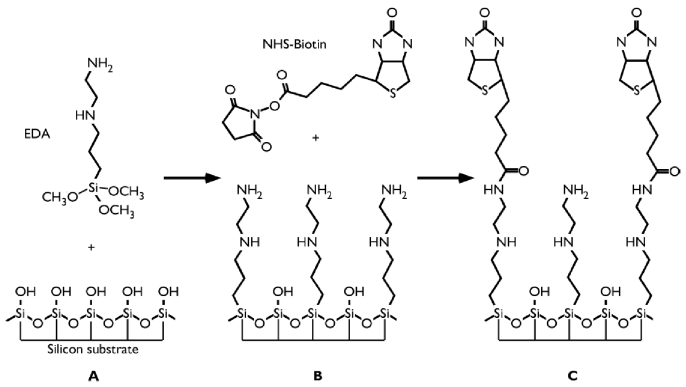

Figure 4.2. Functionalization of a SiO_2 surface in order to display biotin sites. Figure from [19].

4.3 Verification of Immobilization

To make sure that the alkaline phosphatase was *immobilized and active* on the surface the following experiment was carried out.

After the immobilization of the proteins on a piece of silicon oxide wafer, the sample was immersed in a cuvette containing a solution of p-nitrophenyl-phosphate (pNPP) with a concentration of $1\frac{\mu g}{ml}$. Since the reaction product of the dephosphorylation strongly absorbs light at a wavelength of 405 nm, it can easily be measured spectroscopically. For a detailed description of the substrate the reader is referred to section 7.3.

The cuvette was continously stirred and placed every minute into a spectrophotometer in order to measure the concentration of the reaction product. After three minutes the sample was withdrawn from the cuvette and the measurement continued. The experiment was repeated three times. Figure 4.3 shows the result of the three consecutive experiments. In the first experiment (Exp. 1) the slope of the transmission curve remains significantly negative even after the withdrawal of the sample. This suggests that a certain number of proteins *detached* from the sample and went into solution. Repetition of the experiment with the same sample showed however that the detachment happens only once, since the slope after the withdrawal of the sample becomes almost zero (Exp. 2, Exp. 3). This result indicates that apparently some of the proteins on the surface of the sample were not tightly bound but just physisorbed.

As a consequence of this result, the sample was always immersed and stirred in pNPP prior to any experiment that required firmly attached proteins.

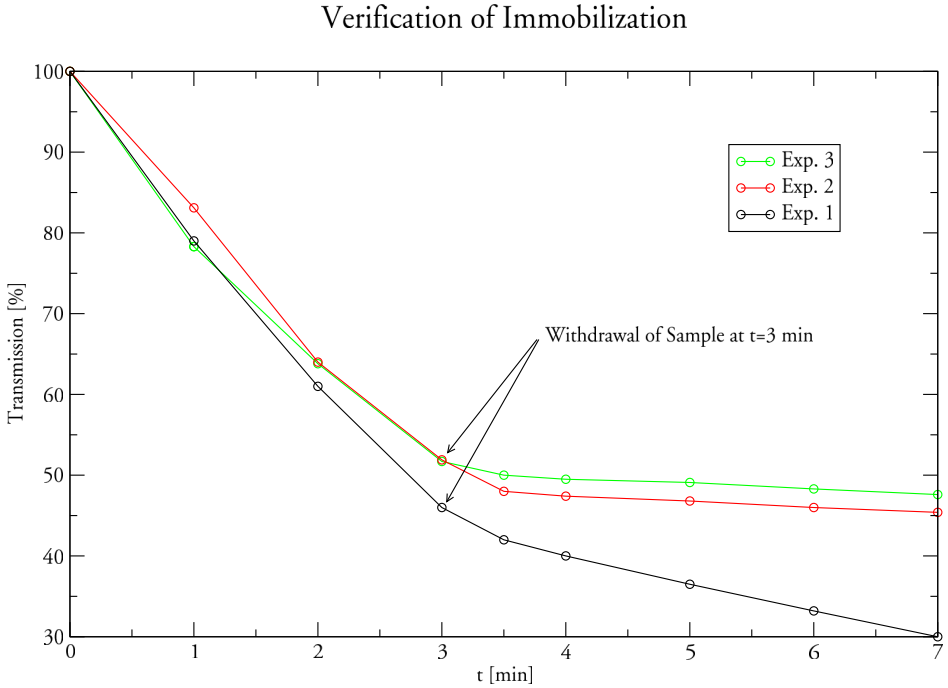

Figure 4.3.

5

Nanolithography

Fourth Law of the Lab:
Experience is directly proportional
to the amount of equipment ruined.

Jeffrey Harrisberger

5.1 Motivation

The idea to "write with proteins" originates from observations in earlier studies by Blank et al.[23]. In these studies single alkaline phosphatase molecules were physisorbed to mica and then exposed to a substrate, which at first is soluble, but becomes insoluble after the enzymatic reaction. As a result, the growth of piles of precipitate around the proteins was observed (Fig.5.1). After a few minutes the growth of the precipitate stopped, which suggested that the proteins buried themselves underneath the reaction product.

This observation lead to the idea that it might be possible "to turn things around" and attach the alkaline phosphatase to the AFM tip, rather than to the support. Having the protein immobilized on the AFM tip would then allow to deposit the precipitate in a controlled fashion.

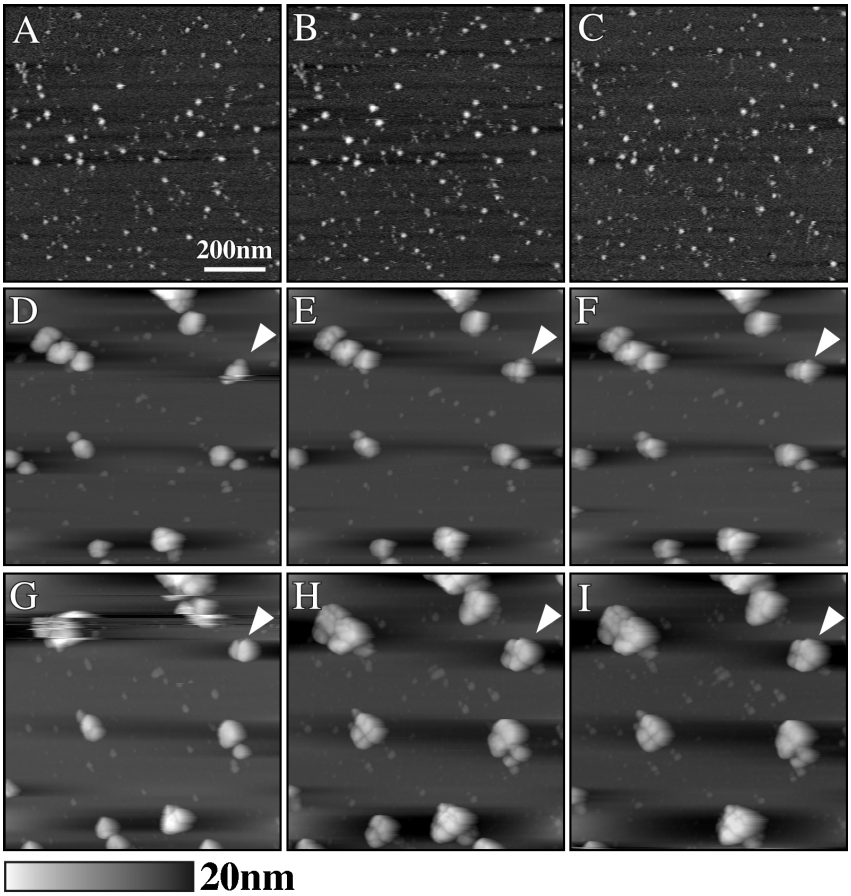

Figure 5.1. The images show the accumulation of precipitate around alkaline phosphatase molecules that have been physisorbed to mica. After the acquisition of image C the surrounding buffer solution was exchanged and replaced with a buffer containing 0.5 mM BCIP/NBT. Subsequently the growth of precipitate around some alkaline phosphatase molecules was observed. The time step between two consecutive images was 2 min. Result by Blank et al [23].

5.2 The substrate BCIP/NBT

In all experiments that relied on precipitation a unique substrate was used. It consists of two components, namely 5-bromo-4-chloro-indoxyl-phosphate (BCIP) as the actual substrate, and the cofactor nitro-blue-tetrazol (NBT). The transition from being soluble to insoluble involves a multi step reaction in which the alkaline phosphatase first dephosphorylates the substrate BCIP, which after dimerization into indigo blue supplies two excess protons. These two protons then reduce the second component NBT to form formazan, which forms a complex with the indigo molecule and then precipitates (Fig. 5.2) [24].

Originally this reaction scheme finds application for phosphatase-based blotting and immuno-histochemistry, because the reaction product is insoluble and of deep purple color.

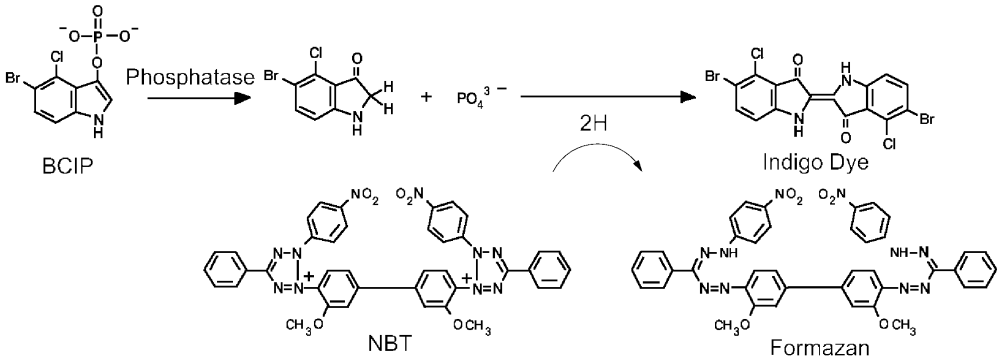

Figure 5.2. The alkaline phosphatase dephosphorylates the substrate BCIP which, after dimerization into indigo blue, supplies two excess protons. These two protons then reduce the second component NBT to form a insoluble complex with the indigo dye.

5.3 A first Attempt

As stated above the idea was to attach the protein to the cantilever in order to control the deposition of the precipitate. Since it is not trivial to attach the protein only to the apex of the AFM, a first attempt was made in which the *complete* cantilever, including the supporting chip, was functionalized with streptavidin-conjugated alkaline phosphatase by the same procedure as described in section 4.2. Although the cantilever is made of silicon-nitride, also silanol groups are present on the surface which allow the covalent attachment of silanes.

The functionalized chip was then installed in the AFM (MFP 3D - Asylum Research) and immersed in a solution containing equal parts of BCIP/NBT and a buffer containing 40 mM TRIS buffer substance and 1 mM $MgCl_2$ at a pH of 9.8.

Since the protein was present on the complete cantilever and chip, the precipitate was produced everywhere along those surfaces. The result was that a large amount of precipitate became present in the solution, which then condensed on the support. Figure 5.3 shows an image of the support obtained in tapping mode. Prior to the image acquisition a rectangular area had been scraped off in contact mode, leaving an area cleared of precipitate.

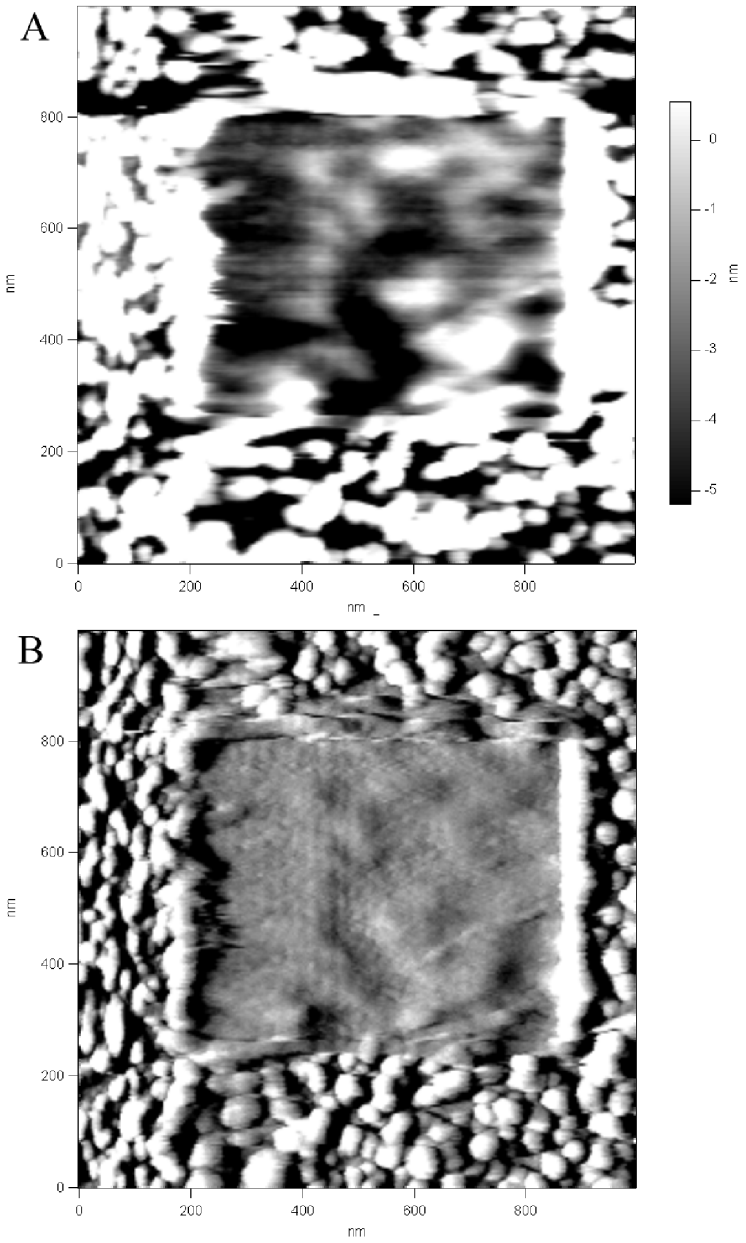

Figure 5.3. Tapping mode image of precipitate condensed on the support. A rectangular area was cleared by scraping in contact mode. Image (A) shows the height, image (B) encodes the amplitude of the cantilever oscillation.

5.4 Immobilization on the Apex of the AFM Tip

The first attempt to do enzyme assisted nanolithography with a fully protein-covered cantilever did not yield a satisfying result. Obviously, the problem was that too much protein was distributed all over the cantilever causing a non-confined and too large production of the precipitate.

To improve the situation a way of immobilizing the protein on the very apex of the AFM tip had to be found. Keeping in mind the miniscule dimension of the AFM tip, with a typical radius of curvature of 15 nm, this is not an easy task.

Since streptavidin exhibits four biotin binding sites, the idea was to first immobilize the streptavidin-conjugated protein on the support by means of the surface functionalization described in section 4.2. In a second step, this support was approached with an AFM tip that was also functionalized in order to display biotin on its surface. Bringing the tip in close contact with the streptavidin then allowed to bind to a vacant biotin binding site. Upon retraction, there then is a certain chance of "picking up" the protein, depending on the number of binding events of the competing sides (Fig. 5.4).

The fact that the employed streptavidin-phosphatase conjugate exhibits a ratio of 2:1, i.e. that on average two streptavidin molecules are bound to one phosphatase molecule, might promote the binding to the AFM tip. If the second streptavidin is not orientated towards the surface it might be more accessible for other binding partners, like the functionalized tip.

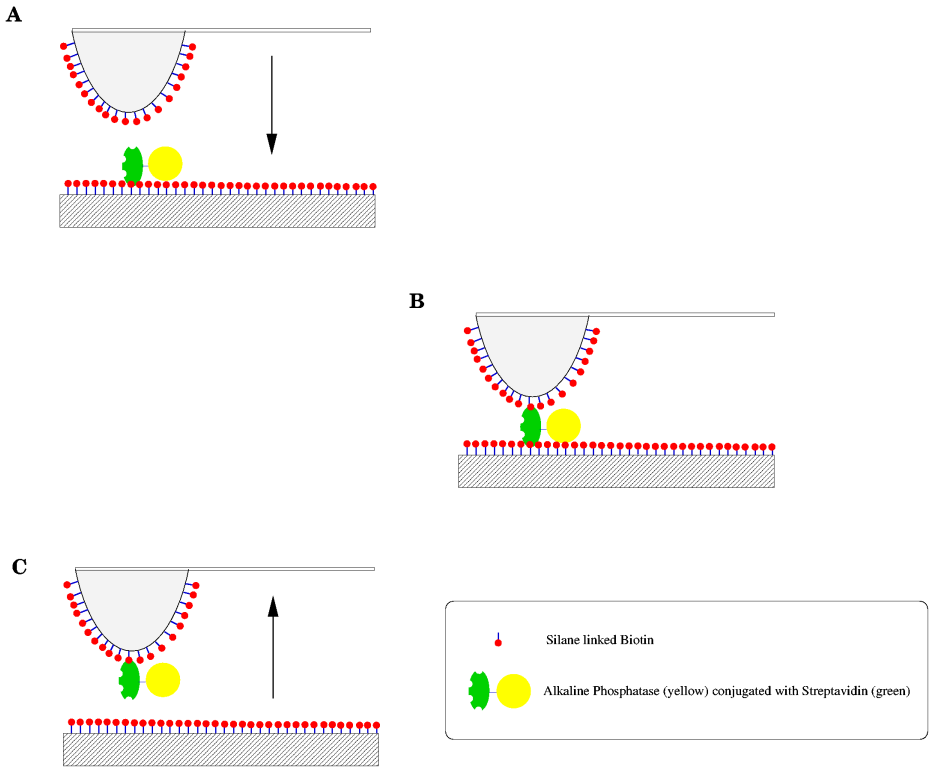

Figure 5.4. "Pick Up" strategy for immobilization on the apex of the AFM tip.

5.5 From Theory to Experiment

In the actual experiment the immobilization of the protein on the apex of the AFM tip was performed by starting out with a surface that was sparsely populated with alkaline phosphatase according to the procedure described in section 4.2. Figure 5.5 shows AFM images of the treated silicon oxide wafer surface. The density of the proteins is roughly 10 $\frac{1}{\mu m^2}$ and the height of the streptavidin-phosphatase-complex is typically 5 nm as indicated in the line-section of Figure 5.5 . In order to avoid premature binding to the biotinylated AFM tip, the imaging was carried out with a non-functionalized AFM tip.

The next step was to immobilize the proteins on the apex of the biotin-functionalized tip. First the chip was installed in the AFM and then engaged in contact mode. Next, it was moved at a relatively slow speed of 1 $\frac{\mu m}{s}$ for a time of 1000 s. During the scanning an area of 4 µm was covered, which corresponds to an approximate number of 40 encounters between the AFM tip and the immobilized proteins.

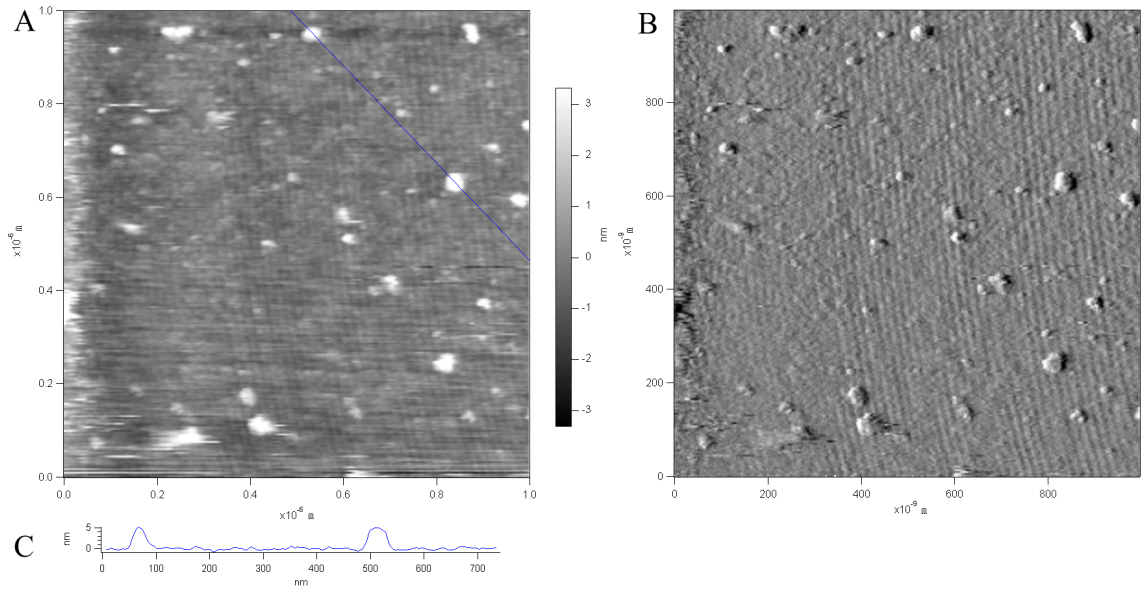

Figure 5.5. This image shows the height (A) and deflection (B) image of single streptavidin conjugated alkaline phosphatases that are immobilized on the oxide layer of a silicon wafer. Part C shows a height trace along the blue line drawn in the height image, indicating a height of roughly 5 nm for single protein complexes .

With the phosphatase-functionalized tip it then was possible to carry out the actual nanolithography experiment. The surface on which the precipitate was supposed to aggregate was chosen to be *mica* [25]. This silicate has some remarkable properties, which make it particularly suitable for AFM studies. Due to its sheet-like structure, in which the sheets are held together only by relatively weak bonds, it is possible to cleave the crystal along these layers, yielding extremely flat and clean surfaces. In practice, the cleaving is done by sticking a piece of duct tape on a piece of mica and then removing

the tape, thus taking away a few of the top layers. For easier handling the piece of mica is glued to a stainless steel plate.

Next, the mica support and the phosphatase-functionalized AFM tip were installed in the AFM and immersed in the substrate solution. It is important to minimize the time the phosphatase-functionalized tip is exposed to the air in order to prevent denaturation of the protein. Since the AFM tip remains installed in the instrument, while exchanging the support, it is possible to prevent the tip from drying by keeping the tip immersed in a droplet of buffer solution that is applied by a pipette. The substrate solution is a 1:1 mixture of two fractions A and B. Fraction A contains 40 mM TRIS buffer and 1 mM $MgCl_2$ at pH 9.8. The B fraction is the stock solution of the substrate BCIP/NBT as provided by the supplier, which contains the BCIP at a concentration of 0.56 mM and NBT at a concentration of 0.48 mM.

Prior to the writing process, the surface is imaged in tapping mode to verify that it is clean. In order to start the actual deposition of the precipitate, the AFM tip is brought into contact with the surface. Although the insoluble reaction product is constantly produced, the actual condensation only takes place when the tip is in contact with the surface. This is due to the hydrophobic effect, which promotes the agglomeration of hydrophobic constituents in an aqueous environment.

5.6 Results

In a first experiment dot-like structures were produced on the mica surface. This was accomplished by bringing the functionalized tip in contact with the surface and remaining there for defined time. Afterwards, the instrument was switched to tapping mode and the area around the anticipated dot was imaged.

The structures shown in Figure 5.6 were produced by touching the surface for 20 s in each spot position before moving on to the next. The deposited precipitate had a typical width of 170 nm and a height of about 10 nm.

It also proved to be possible to produce continuous structures by moving the tip over the surface while in contact. Figure 5.7 depicts a structure that was created by moving the engaged tip with velocity of 10 $\frac{\mathrm{nm}}{\mathrm{s}}$. Again, the size of the features has a typical width of 150-170 nm and a height of about 10 nm. Both the dots and the continuous pattern were created during the same experiment on different locations on the sample.

It turned out that distinct structures were only produced after the substrate solution had been concentrated by thermal evaporation by an estimated factor of 5 to 10. This indicates that the catalytic reaction is diffusion limited. This effect will be discussed more quantitatively in section 5.7.

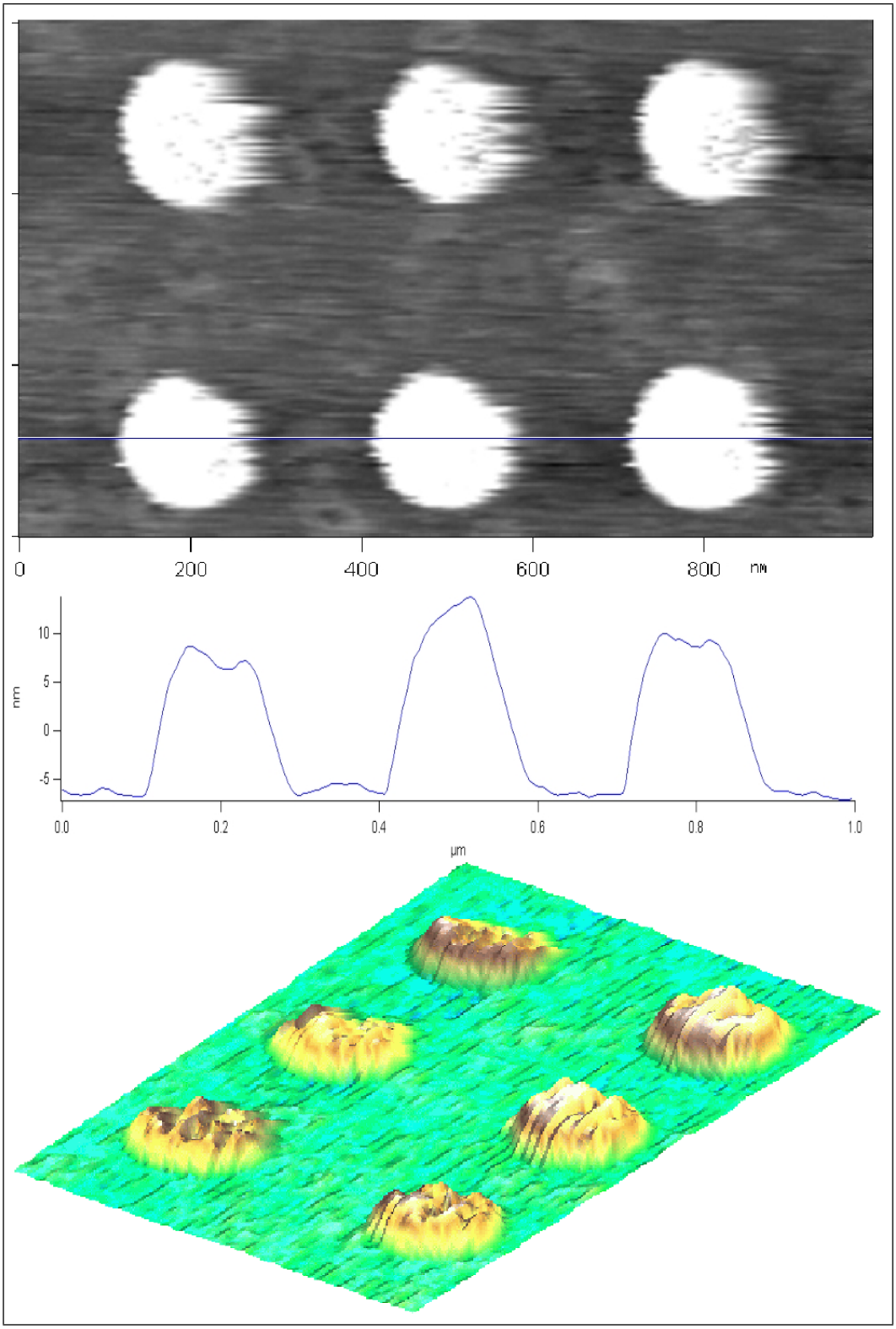

Figure 5.6. This figure shows dots of precipitate that were formed after bringing the alkaline phosphatase functionalized tip in contact with the mica support. For each spot the AFM tip was held in place for 20 s and then moved to the neighboring site. As depicted in the line-section the dots have a typical width of 150-170 nm and a height of 10 nm.

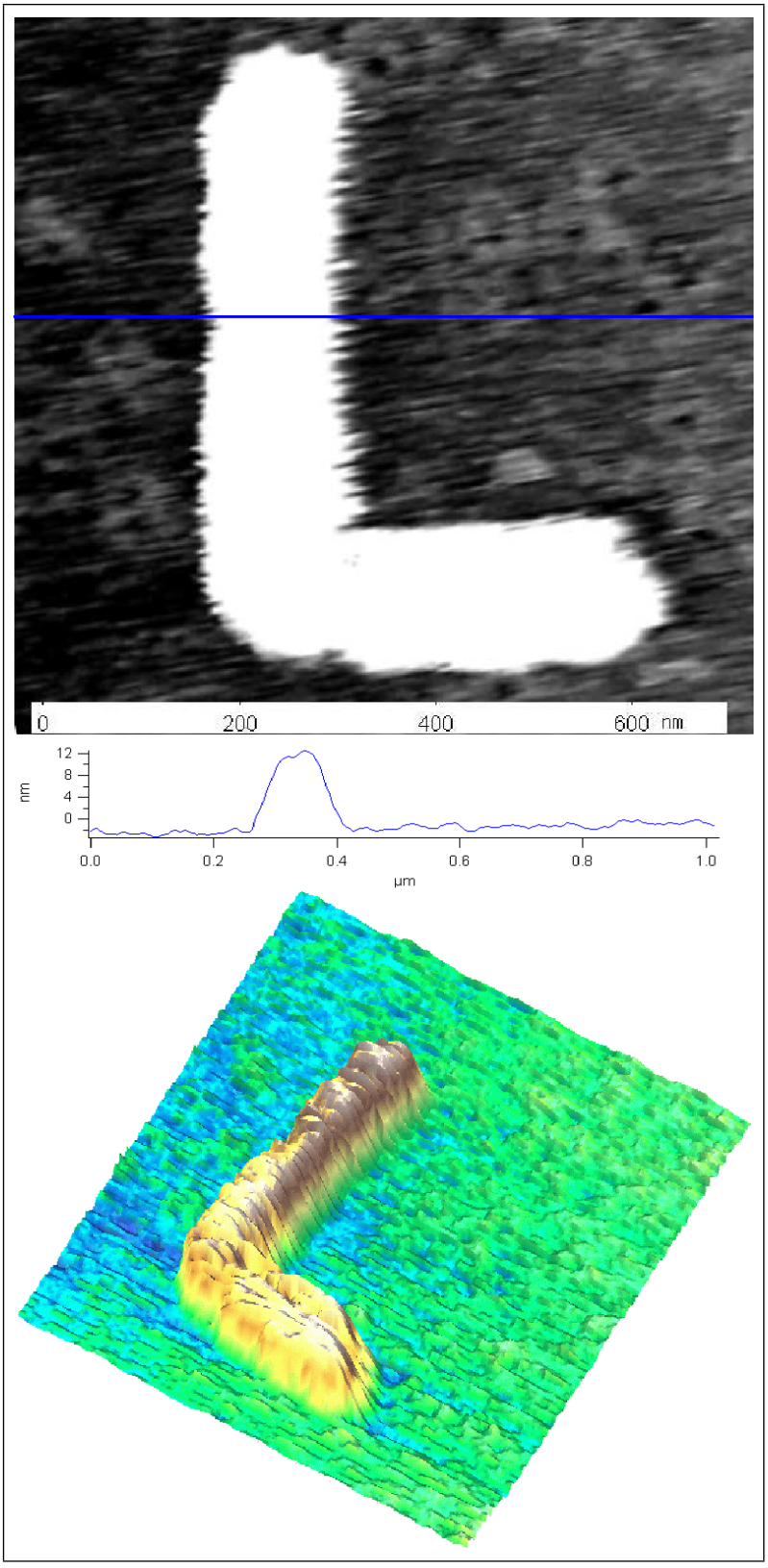

Figure 5.7. This figure shows the deposition of precipitate in a continuous structure. The structure was "written" in contact at a velocity of 10 $\frac{\text{nm}}{\text{s}}$. As depicted in the line-section the structure has a typical width of 150-170 nm and a height of 10 nm.

5.7 Discussion

The achieved results demonstrate the feasibility of producing nanolithographic patterns by employing a small number of proteins that are immobilized on the apex of an AFM tip.

A few problems had to be solved in the development of this method. This includes the immobilization of proteins on SiO_2 surfaces, while retaining their functionality, and the invention of the technique for the confined immobilization of the proteins on the very apex of the AFM tip.

The binding via streptavidin-biotin proved to be a successful and versatile strategy for the immobilization. The problem of localizing the proteins on the apex of the tip was solved by "picking up" the proteins. Only the development of this technique made these experiments possible.

It is important to note that the substrate concentration must be high enough to produce a sufficient amount of precipitate for the deposition. As mentioned above the proper production of patterns became only feasible after the substrate solution had been concentrated by a factor 5-10 due to thermal evaporation.

To understand this effect better an estimation of the reaction rates for the present system will be made. For the sake of simplicity it is assumed that one immobilized proteins is present. The substrate should have a concentration of 0.28 mM and it should acts as a single reactant, meaning that secondary reactions that lead to the actual precipitate are ignored.

A concentration of 0.25 mM BCIP/NBT in water corresponds to one substrate molecule in $2 \cdot 10^5$ molecules of H_2O, which in turn corresponds to 1 substrate molecule in a cubic box of water with the length of the edge of 20 nm.
Since we have to consider diffusion, we will use the following relation

$$t = \frac{r^2}{D} \tag{5.1}$$

in which r is the distance a particle travels on average during time t for a given diffusion constant D. For small molecules in water, such as BCIP/NBT, a diffusion constant of $10^{-10} \frac{m^2}{s}$ can be assumed.

We are interested in the time that a substrate molecule needs on average to diffuse a distance of 20 nm, which is the average distance between a substrate molecule and the protein. From equation 5.1 we find that this time is about 4 µs and it corresponds to an average velocity of the substrate molecules of $v_d = 5 \cdot 10^{-3} \frac{m}{s}$.

In this velocity v_d we are interested, because it it possible to draw an analogy between an ideal gas and solutions of low concentrations. In the kinetic theory of ideal gases a property called *collision frequency* is defined as the frequency at which the atoms of the gas collide. The atoms have a certain collision cross section, which is related to their size. From a geometric argument it follows that the collision frequency is given by

$$z = \sigma \cdot v_d \cdot \frac{N}{V} \tag{5.2}$$

in which z is the collision frequency, σ is the collision cross section and N is the number of atoms per volume V. We assume that the substrate and the active site of the protein have the same collision cross section of $\sigma = 1\,\mathrm{nm}^2$. Using the earlier estimated diffusion velocity of $v_d = 5 \cdot 10^{-3} \frac{m}{s}$ and the number density that corresponds to the 0.25 mM substrate concentration, a collision frequency of $625 \frac{1}{s}$ is calculated from this equation.

This is a low value, especially when considering the potential turnover rate of the alkaline phosphatase of $4200\ \frac{1}{s}$ that the manufacturer states.

Figure 5.8 depicts calculated collision frequencies with their dependence on an increasing substrate concentration. It supports the experimentally made observation that in order to utilize the full enzymatic capacity of the alkaline phosphatase, the substrate concentration has to be high enough.

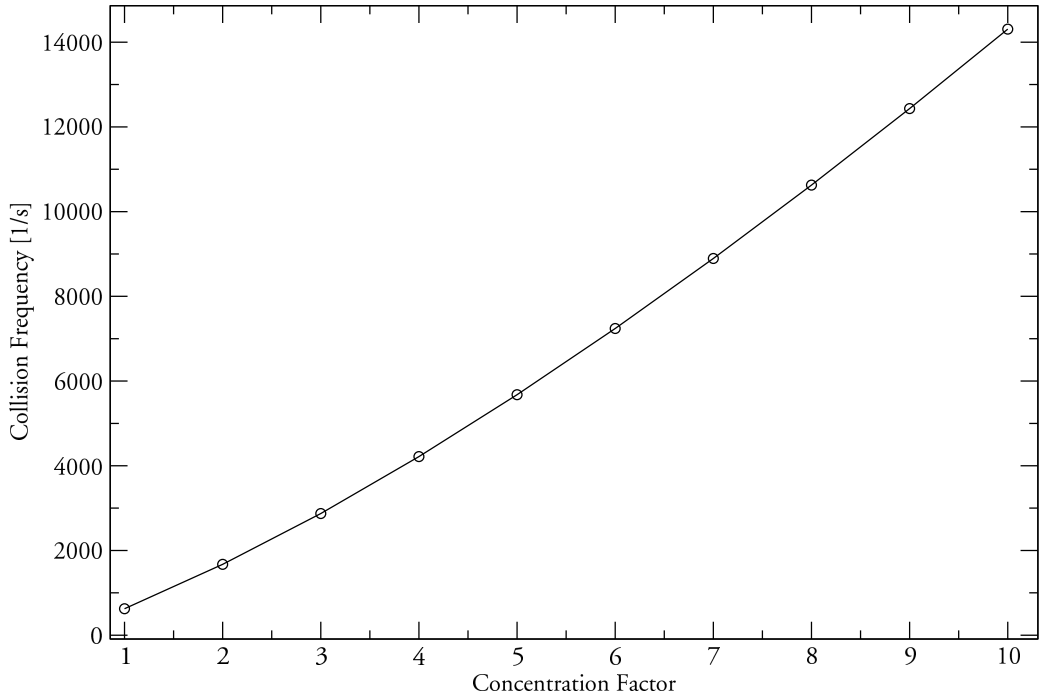

Figure 5.8. Dependence of the collision frequency between protein and substrate on the substrate concentration.

One has to be aware of the fact that this model is a crude approximation that ignores the real complexity of the precipitation reaction with its multiple reaction steps. Another simplification is that any geometric constrains that could influence the diffusion, like the AFM tip and the surface, are ignored.

An additional factor that would demand higher substrate concentrations could be the fact that the substrate gets depleted and that its concentration does not recover fast enough. This could be even more the case if a relatively large number of proteins is closely packed, as it is the case for the functionalized AFM tip used in the experiment.

Diffusion could also be responsible for the relatively large feature size of 150-170 nm because the insoluble reaction product will diffuse some distance before it condensates.

5.8 Conceivable Modes of Operation

The method developed in this work is not limited to the presented realization, but can potentially be adapted to numerous different protein-substrate systems. For example does the substrate not need to be in solution, but can rather be immobilized on a support where it is directly modified by the proteins. More complex reaction schemes, involving additional cofactors, are imaginable as well. Figures 5.9-5.12 illustrate a selection of conceivable setups.

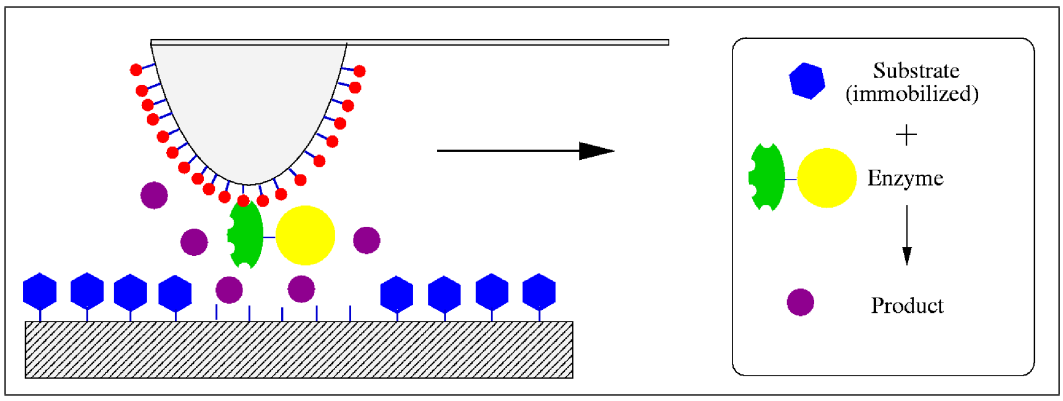

Figure 5.9. The substrate is immobilized on the surface and becomes soluble after the enzymatic reaction. The remaining surface has different chemical or physical properties.

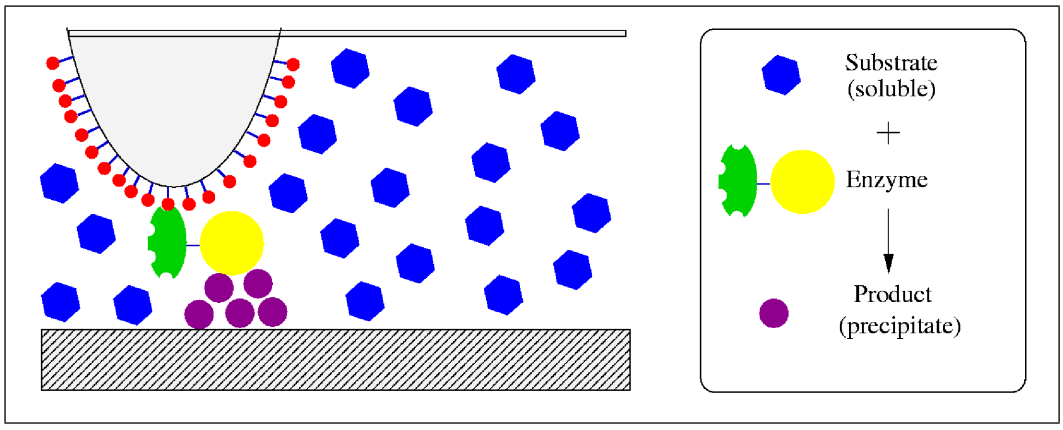

Figure 5.10. The substrate is present in the surrounding medium and becomes insoluble after the enzymatic reaction. By controlling the tip's position, the precipitate may be deposited as desired. This mode is implemented in this work.

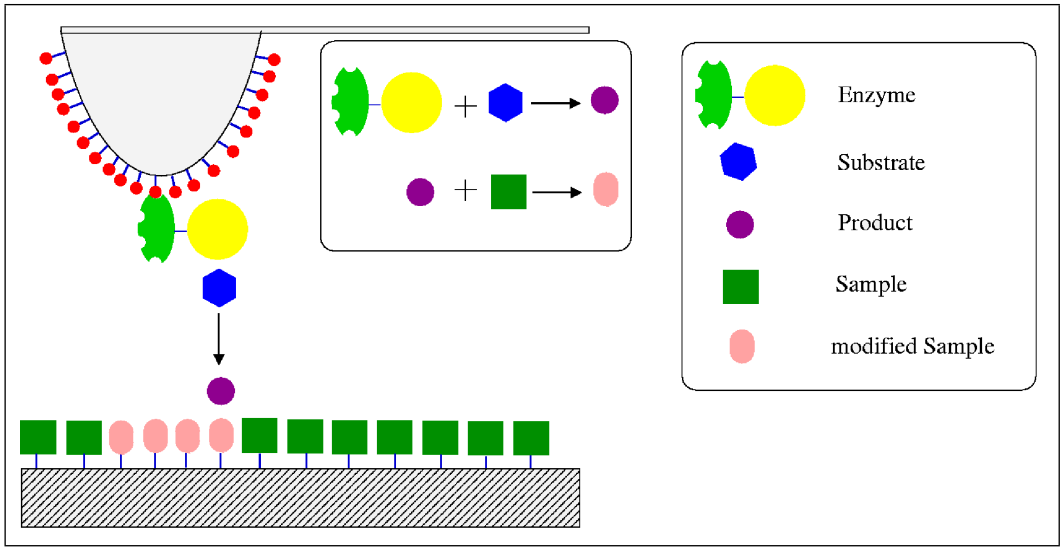

Figure 5.11. The substrate is present in the surrounding medium and the soluble reaction product modifies the molecules that are present on the surface chemically.

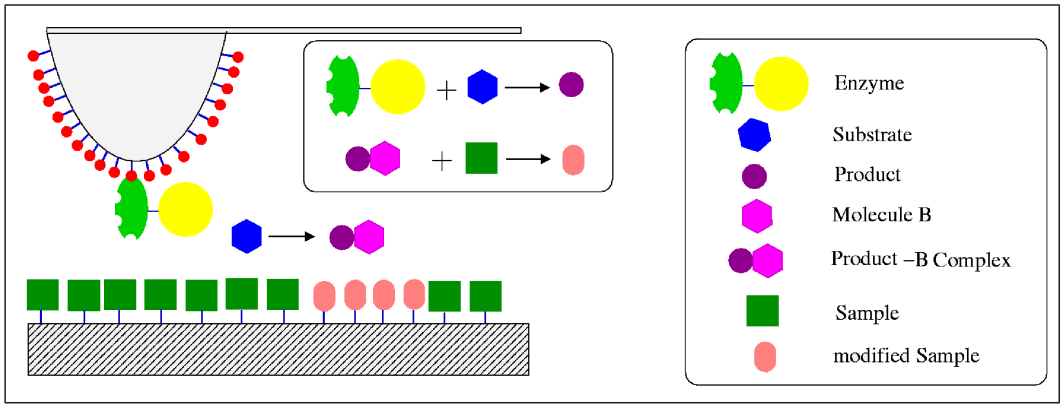

Figure 5.12. The substrate is present in the surrounding medium and the soluble product reacts with a cofactor which then modifies the surface chemically or physically.

5.9 Outlook

So far the feasibility of enzyme assisted nanolithography has been demonstrated. There still is a lot of room for future implementations and optimizations of this technique. The list of further topics to investigate includes:

- **Improving the spatial resolution of the method**

  The most important improvement to the technique described in this chapter is to increase the spatial resolution. Since the results obtained so far suggest that the number of immobilized proteins on the apex of the AFM tip is of the order of 40, thus contributing to the large size of the produced structures, the most apparent improvement would be to decrease the number of attached proteins. Increasing the velocity at which the tip is moved and varying the substrate concentration should also have an impact on the feature size.

- **Reducing the number of immobilized proteins on the apex of the AFM tip**

  The highest priority should have the attempt to reduce the number of involved proteins, ideally to one single active protein. This could be accomplished by decreasing the number of encounters between the biotinylated AFM tip and the proteins that are immobilized on the support simply by decreasing the covered area while scanning the surface. Since this method does not allow to quantify the number of picked up proteins the following approach might provide a solution.

- **Image – Select – Pick Up – Verify**
  The idea is to image the immobilized proteins prior to picking them up in *Tapping Mode*, assuming that the interaction between the functionalized tip and the protein is so weak that no binding will take place. After selecting a target protein the scan range will be confined around this one molecule, which then can be picked up in *Contact Mode*. After retrieval of the single protein a second scan in *Tapping Mode* can verify the detachment from the surface. This method would allow to have full control over the number of immobilized proteins.

- **Employing different proteins**
  The realization of nanolithography in this work served basically as a prove of concept to show that it is possible to immobilize a small number of proteins on the apex of an AFM tip in order to locally modify a support. Since the binding via streptavidin conjugation is a generally applicable method, basically any protein is viable to be employed. This fact opens the possibility to choose from the enormous amount of different proteins with all their unique functions, which gives this technique a “toolbox” character.

- **Obtaining electron microscopic or AFM images of tip with proteins**

  It should be possible to verify and eventually even quantify the number of immobilized proteins on the apex of an AFM tip by either electron microscopy or direct AFM imaging of the pyramidal tip. In the case of electron microscopy the use of a streptavidin-gold conjugate might improve the detectability.

- **Generating 3-dimensional structures**

  A very challenging idea is to produce 3-dimensional structures. This might be feasible in analogy to photo-induced polymerization, a technique in which a focused laser beam induces a polymerization reaction in a solution, which allows a 3-dimensional structure to be progressively build up. This method is used to prototype arbitrary shaped compounds with typical sizes of a few cm or decimeter.

  The idea is to improve the spatial control over the polymerization by a few orders of magnitude. This might be done by utilizing an appropriate protein that would be immobilized on an AFM tip in order to induce the polymerization in a suitable substrate on a much smaller scale.

  This is just brainstorming and has to be taken with a grain of salt.

- **Regulating the protein activity**

  In order to get even more control over the modification process, it would be desirable to be able to deliberately regulate the protein activity. The activity of proteins depends on a variety of factors such as temperature, pH, the presents of cofactors, allosteric effects and the availability of energy sources such as ATP or ion gradients. If it would be possible to externally modify an appropriate factor in a controlled fashion, the protein activity could be regulated. The next section will deal with an attempt to do this by trying to change the pH of the nearby environment of the protein.

- **Modifying the viscosity of the substrate solution**

  It would be beneficial to get a better understanding of the involved diffusion processes. This applies to the diffusion of the substrate as well as to the diffusion of the reaction products, since it can be the limiting factor for the spatial resolution and for the velocity at which modifications can be carried out. A simple approach to increase the viscosity of the medium would be the addition of glycerine.

Part II

Attempt to Control Protein Activity with Surface Potentials

6

Theoretical Background

We are all agreed that your theory is crazy. The question which divides us is whether it is crazy enough to have a chance of being correct. My own feeling is that it is not crazy enough.

Niels Bohr

6.1 Introduction

To have better control over surface modifications by proteins that are immobilized on an AFM tip it would be favorable to regulate the protein activity deliberately. The activity of proteins depends on a variety of factors such as temperature, pH, the presents of cofactors, allosteric effects, the availability of energy sources such as ATP or ion gradients. From this list, the factor that can be most easily influenced is the pH in the vicinity of a protein that is immobilized close to an electrically conductive surface.

The pH of a solution will be shifted close to an *electrically charged surface* due to the alteration of the ionic environment. The details of this phenomenon will be discussed in section 6.3. Since the electric surface potential can be adjusted by an external voltage it is possible to modify the pH in the vicinity of the surface. Figure 6.1 illustrates this idea, in which the red color indicates the pH of the solution. In state A the solution is kept at a pH at which the protein activity is reduced, whereas in state B an external electrical potential is applied, which results in a shift of the pH in the vicinity of the surface. If the external potential is chosen appropriately the pH can be shifted to an optimal value to promote the protein activity.

Even though this concept should work in principle, it failed to work in practice so far. In order to understand why, some theoretical background is necessary, which is given in this part of the work. Additionally, an experiment for detecting the influence of an external electric potential to the protein activity will be described and suggestions will be given for an eventually more adequate experiment in the future.

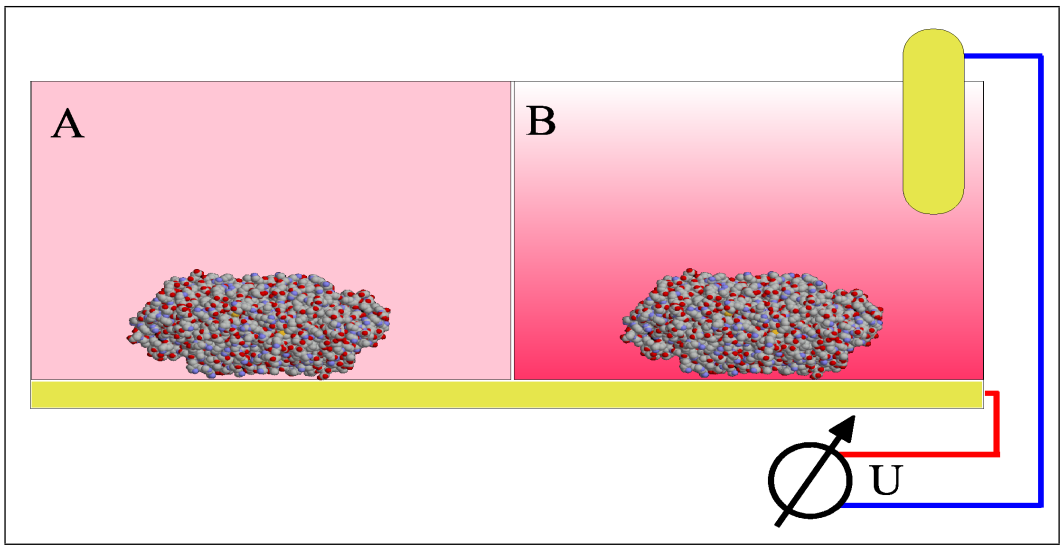

Figure 6.1. Applying an electric potential changes the pH in the vicinity of the charged surface.

6.2 The pH Dependence of Protein Activity

Proteins generally show a dependence of their activity on the pH of the surrounding medium. This behavior originates from the fact that aminoacids will be ionized in an aqueous solution. The state of ionization (cationic, zwitterionic, anionic), which depends on the pH, influences the conformation and the chemical properties of the active site and consequently the activity of the protein.

Figure 6.2 shows the pH dependent activity of the alkaline phosphatase employed in this work. Details on the photometric assay that was used to determine this dependence are found in section 7.4.

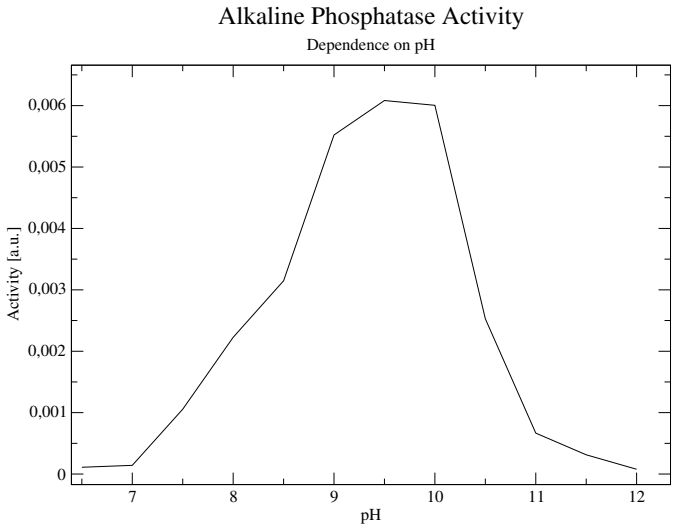

Figure 6.2.

6.3 The Spatial Distribution of Surface Potential

Ionic solutions containing positive and negative ions experience an alteration of the ion distributions in the presents of an electrically charged surface. The spatial distribution of the electric potential was already modeled in 1910 by Gouy and Chapman [26], assuming a planar and uniformly charged surface.

The derivation of the electric potential $\phi(x)$ is based on two assumptions. Firstly, the Poisson equation:

$$\nabla^2\phi = -\frac{\rho}{\epsilon\epsilon_o} \tag{6.1}$$

in which ϕ is the electric potential, ρ is the charge density, ϵ_o is the permittivity constant and ϵ is the dielectric constant of the medium. Secondly, the assumption that the probability of finding an ion at some point from the surface follows the Boltzmann distribution:

$$n^+(x) = n_o \cdot exp\left(-\frac{ze_o\phi(x)}{kT}\right) \tag{6.2}$$

$$n^-(x) = n_o \cdot exp\left(+\frac{ze_o\phi(x)}{kT}\right) \tag{6.3}$$

in which n_+ and n_- are the respective concentrations for positive and negative ions assuming a positively charged surface, n_o is the ion concentration of the undisturbed solution, z is the valency of the ionic species, e_o is the electronic charge, k the Boltzmann constant and T the temperature of the system.
Substituting the equations for the charge density Eq. 6.2 and Eq. 6.3 into the Poisson equation Eq. 6.1 yields the so called Poisson-Boltzmann equation:

$$\nabla^2\phi = -\frac{ze_on_o}{\epsilon\epsilon_o}\left[exp\left(-\frac{ze_o\phi(x)}{kT}\right) - exp\left(+\frac{ze_o\phi(x)}{kT}\right)\right] \tag{6.4}$$

Assuming the boundary conditions $\phi(x \to \infty) = 0$ and $\phi(0) = \phi_o$ the solution of this differential equation is:

$$\phi(x) = 2\frac{kT}{ze_o}ln\left(\frac{1 + e^{-\kappa x}tanh(ze_o\phi(0)/4kT)}{1 - e^{-\kappa x}tanh(ze_o\phi(0)/4kT)}\right) \tag{6.5}$$

with the equivalent form:

$$tanh\left(\frac{ze_o\phi}{4kT}\right) = tanh\left(\frac{ze_o\phi(0)}{4kT}\right) \cdot e^{-\kappa x} \tag{6.6}$$

For small $\phi(x)$ the relation $tanh(\phi) \approx \phi$ holds, thus

$$\phi(x) = \phi(0) \cdot exp(-\kappa x) \tag{6.7}$$

The variable κ^{-1} has the units of a length and its value denotes the distance at which the potential has decayed to the e^{-1} fraction from the value at the surface. This so called the Debye[1] length can be approximated for a monovalent solution by $\kappa^{-1} = 0.294/\sqrt{c}[\text{nm}]$, in which c is the molar ion concentration.

An important limitation results from the assumption of point charges and the neglect of real ionic diameters. For small values of κx equation 6.3 yields unrealistically high concentrations near the surface. In order to improve this condition, Stern [27] suggested to divide the double layer close to the surface in two regions. One should consist of counter ions adsorbed directly to the surface (Stern layer), the other consisting of the Gouy-Chapman layer. Figure 6.3 illustrates the ion distribution and the associated potentials.

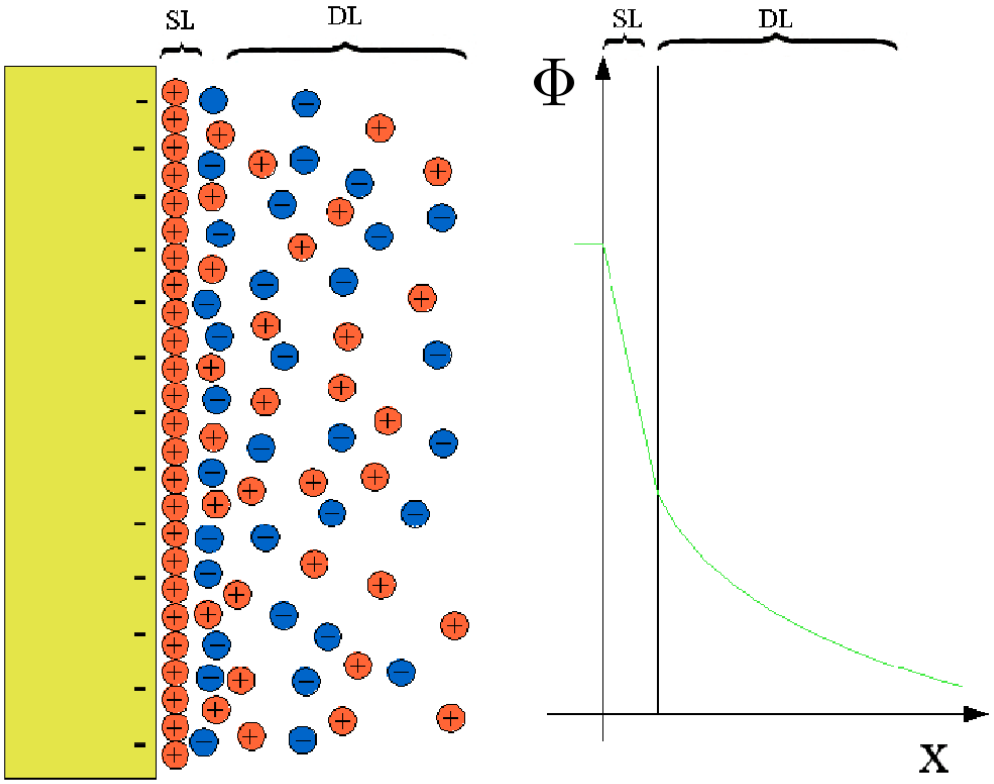

Figure 6.3. Distribution of ions and the associated electric potential close to an electrically charged surface. The so called Stern layer (SL) consists of a layer of counter ions that are adsorbed to the surface which cause a linear drop of the surface potential. The diffuse layer (DL) shows the exponential decay of the electric potential as described by the Gouy-Chapman theory.

[1] Peter Debye 1884 – 1966

6.4 The Relation between Surface Potential and pH

The pH value defines the proton concentration of a solution as:

$$pH = -\log_{10}\left[H^+\right] \tag{6.8}$$

Recalling that the concentration of an ionic species is depended on the electric potential of a charged surface (Eqs. 6.2, 6.3) it is possible to relate this surface potential to a *shift* of the pH. Normalizing Eq. 6.2 yields:

$$\frac{n^+}{n_o} = exp\left(-\frac{ze_o\phi(x)}{kT}\right) \tag{6.9}$$

which when substituted in Eq. 6.8 results in:

$$\Delta pH = -\log_{10}\left[exp\left(-\frac{ze_o\phi(x)}{kT}\right)\right] \tag{6.10}$$

Equation 6.10 allows to relate the shift of the pH at a certain distance from the surface to the surface potential.

Figure 6.4 depicts the exponential decay according to Eq. 6.5 for varying surface potentials in the case of deionized water. Due to the carbon dioxide contents of the air, which causes a slight pH change of the water exposed to it, the concentration of H^+ ions was assumed to be $1.6 \cdot 10^{-6}$ M which corresponds to a Debye length of D_L=275 nm and the pH 5.8.

As a consequence of this large value for D_L the screening effect on charges is relatively small, which results in significant potentials still being present 10 nm away from the surface (Fig. 6.4). The absolute value of the associated pH shift according to equation 6.10 is plotted in Figure 6.5. At a distance of 10 nm it still is possible to induce a pH shift of four pH units.

It is important to note, that the values for the electric potential and the pH shift at distances smaller that 2.5 nm have to be considered unphysically high due to the neglect of ionic diameters in the Gouy-Chapman model. The 2.5 nm distance is indicated by the dotted line.

The decay of the electrostatic potential is a strong function of the Debye length (κ^{-1}), which in turn is related to the ionic concentration. For a 1 mM solution of monovalent ions the potential decays much faster than that in deionized water. Figure 6.6 depicts the decaying electrostatic potential and Figure 6.7 the associated pH shift for the 1 mM solution.

Comparing with the results for deionized water reveals that the electric potential falls off more rapidly and that the achievable pH shift at a distance of 10 nm is around 0.5-1 pH units as compared to 4 pH units. For better comparison both cases are presented combined in Figure 6.8

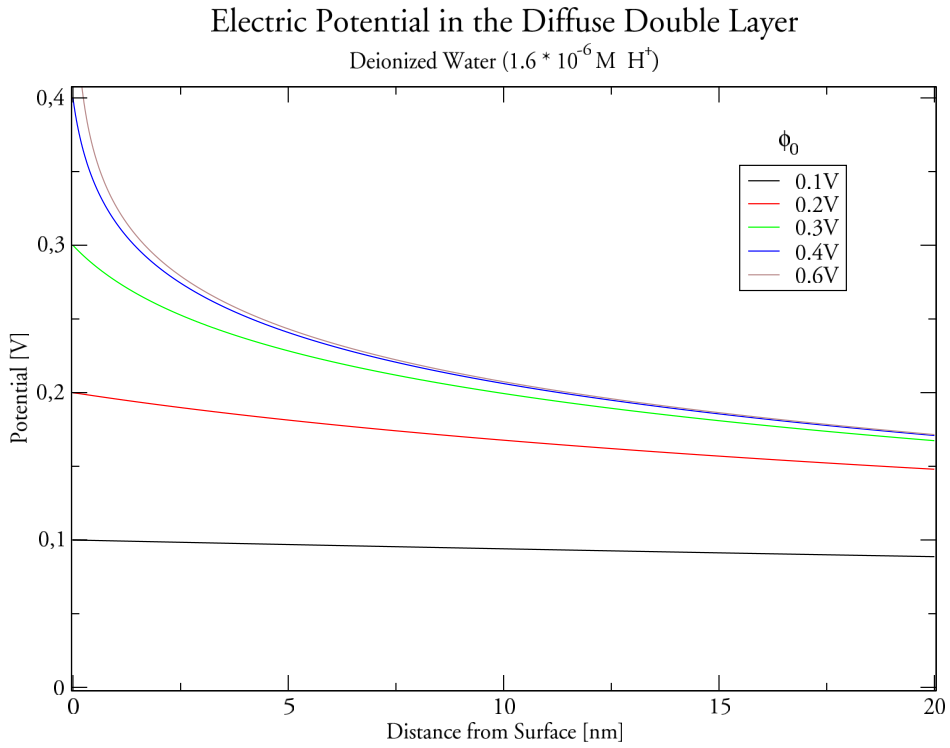

Figure 6.4.

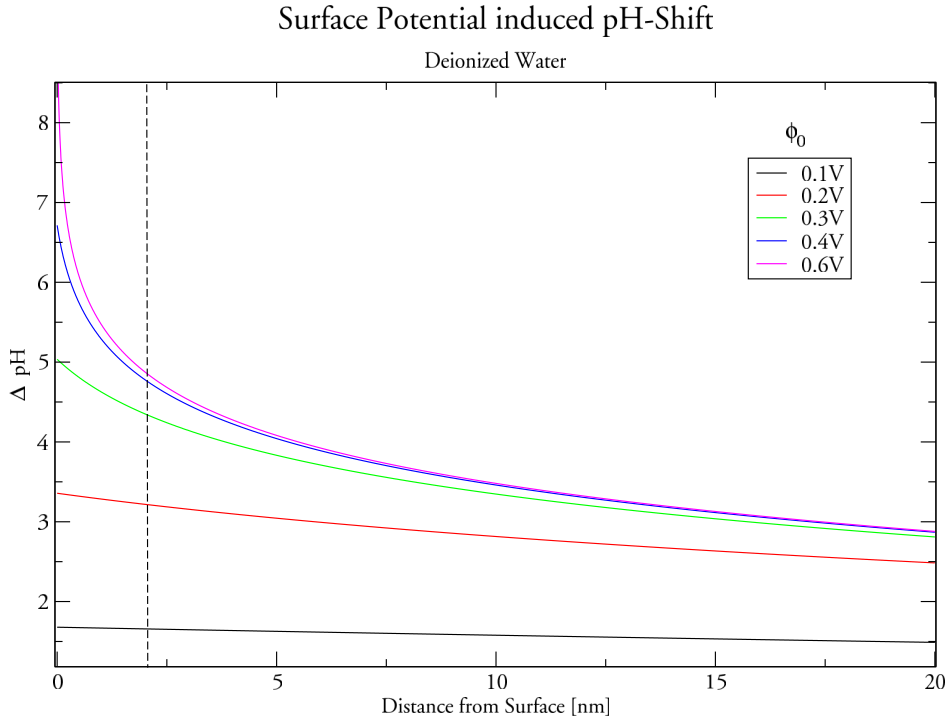

Figure 6.5.

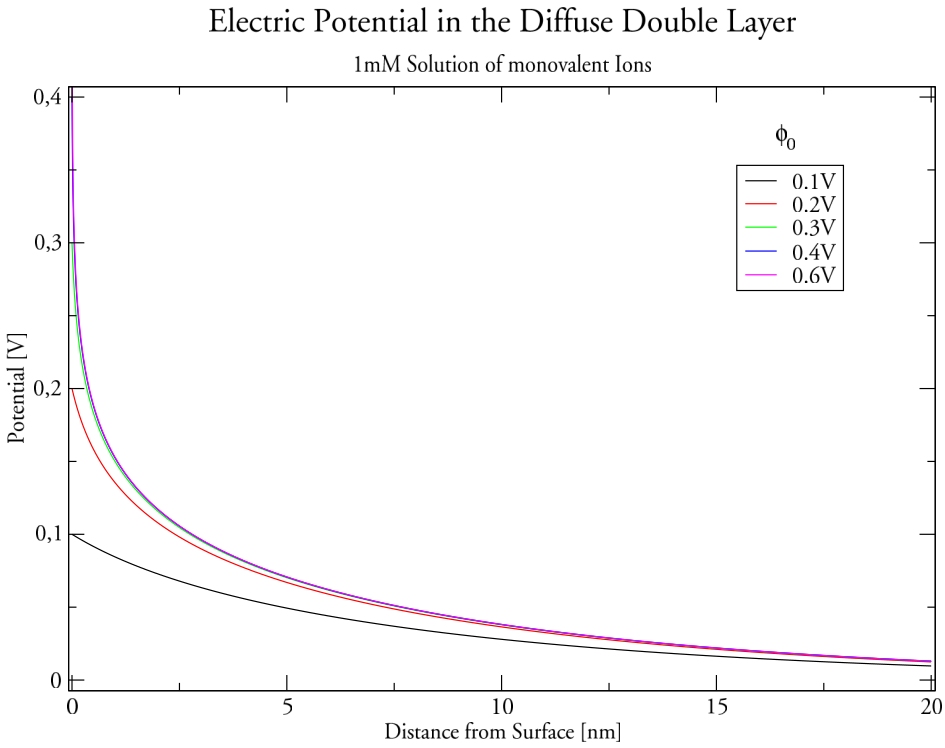

Figure 6.6.

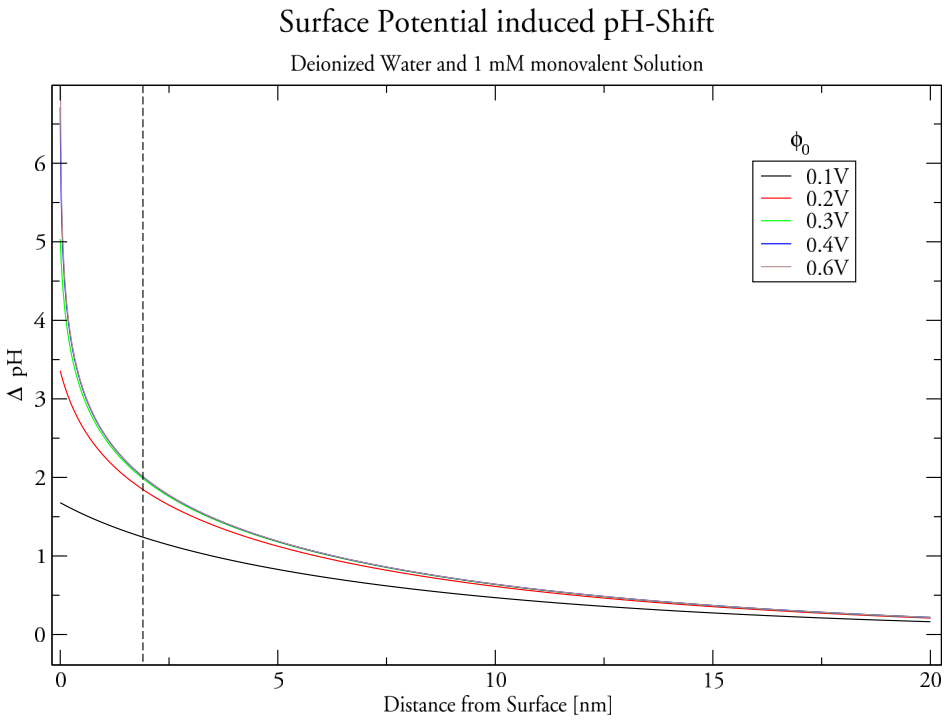

Figure 6.7.

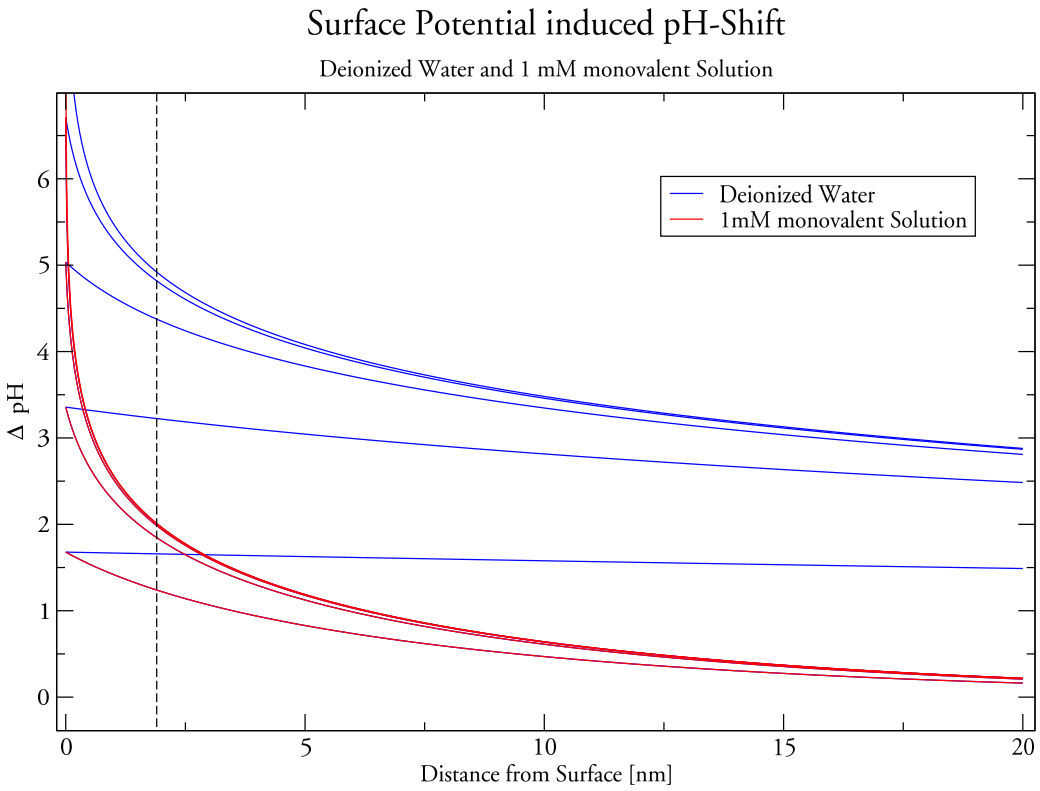
Surface Potential induced pH-Shift
Deionized Water and 1 mM monovalent Solution
Deionized Water
1mM monovalent Solution
Δ pH
Distance from Surface [nm]
0
1
2
3
4
5
6
0
5
10
15
20

Figure 6.8.

6.5 Buffer Capacity of Proteins and Substrate

Proteins

When dealing with the change of pH values one has to consider the buffer capacity of the molecules involved in the process. In the present case these molecules are the alkaline phosphatase, the substrate with its reaction products and eventually a buffer substance like TRIS.

Aminoacids exhibit an amphiprotic behavior, meaning that they have characteristics of both an acid and a base. This is due to the ionizable carboxylic- and the amino groups that are present in any aminoacid. Figure 6.9 depict the titration curve for the aminoacid glycine. The flat parts of the curve around pH 2 and pH 10 indicate the buffer capacity of the aminoacid that is due to the deprotonation of the carboxylic- and the amino group [28].

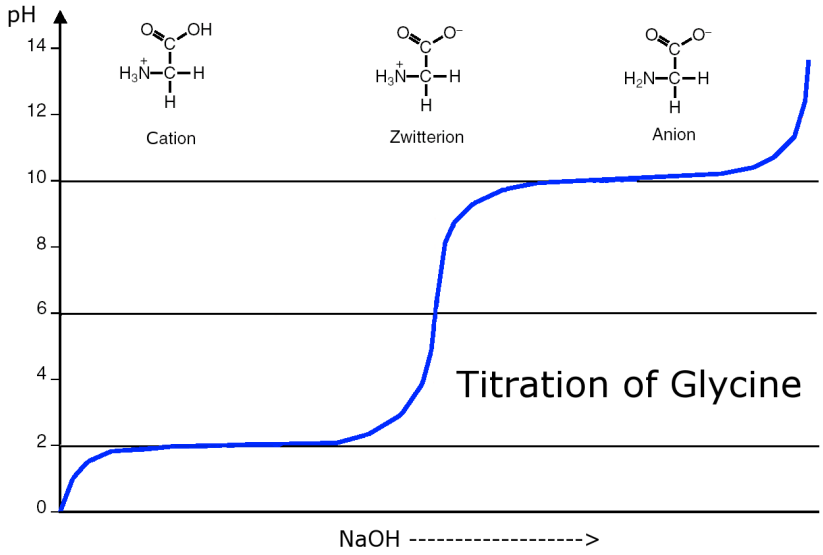

Figure 6.9.

Substrate

Also the substrate used in this experiment with the short name pNPP (details are found in section 7.3) exhibits a buffer capacity. It is especially true for this substance because its hydrolysis releases a phosphate ion. This phosphate is capable of accepting three protons, which results in plateaus in the titration curve around pH 2.1, pH 7.2 and pH 12.3.

The buffer capacity of proteins and substrate might be significant to the failure of regulating the protein activity with surface potentials. A more quantitative analysis of the effects of buffers would be favorable but is beyond the scope of this work.

7

The Experiment

A couple of months in the laboratory
can frequently save a couple of hours in the library.

Anonymous

7.1 Introduction

After giving a theoretical background on the properties of electrical surface potentials the experiment will be described that was carried out in the attempt to detect the anticipated regulative effect.

The difficulty with measuring the activity of proteins that are immobilized on a surface is that the reaction products will stay in the vicinity of the surface and only slowly diffuse into the bulk of the solution. Experiments in an ordinary spectrophotometer, in which the bottom of a cuvette had been replaced with a functionalized surface, proved to be unemployable. This problem demanded a different approach.

The answer was to let the light beam for the measurement of the absorption pass through the substrate solution and let it then *reflect* on the functionalized surface before being detected. Figure 7.1 illustrates this idea. Since ordinary photometer do not provide such a mode of operation, some creativity was necessary.

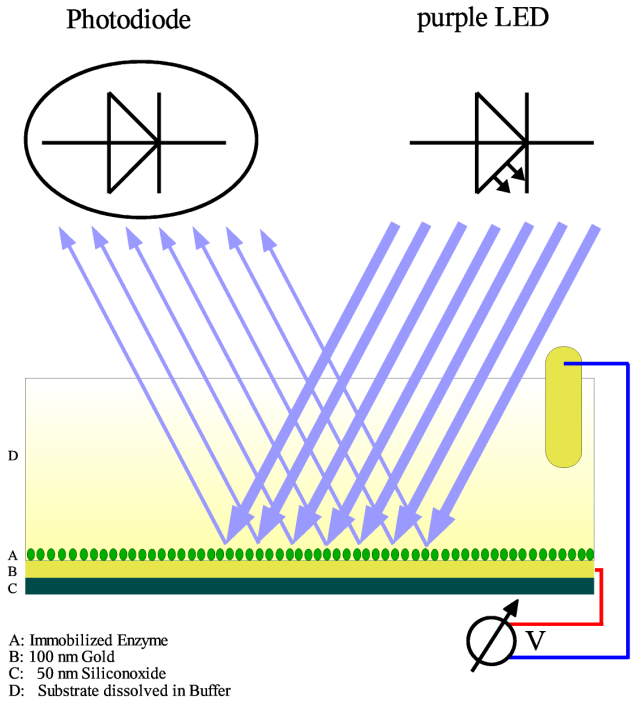

Figure 7.1. Schematics for the measurement of the absorption through the entire substrate solution.

The idea was to modify a prototype AFM head, which was part of the self-built AFM project. This component had become unused and was available for modifications. Details of the AFM project will be discussed in part III.

If operated as an AFM the laser beam takes a beam path as indicated in Figure 7.2. The laser is mounted in position (A) and shines onto a slanted mirror (B) which reflects the beam downward onto the cantilever (C). The reflected beam then hits another rotatable mirror (D) which reflects the beam onto a quadrant photo diode (E).

By replacing the laser with a LED, it was possible to produce a wide beam (⌀ 14 mm) in position (C). This wide beam then passes through the sample cell (C). The reflected beam then falls onto the rotatable mirror (D) which is adjusted properly in order to provide the maximum intensity on the quadrant diode (E). The detected signal is then sampled by a computer at a rate of 10 Hz.

To observe the absorption of the reaction product it was necessary to use light at the correct wavelength. It turned out that the absorption maximum for the pNPP substrate coincides almost perfectly with the emission maximum of a regular purple LED. Figure 7.4 shows a typical emission spectrum of such a LED. With this setup it was possible measure the absorption with high sensitivity.

To avoid undesired buffering effects and to attain a large Debye length, the use of a buffer substance such as TRIS was set aside. Also no $MgCl_2$ was added which usually promotes the activity of the phosphates. Standard photometric assays showed, that even in deionized water the phosphatase retains a significant activity.

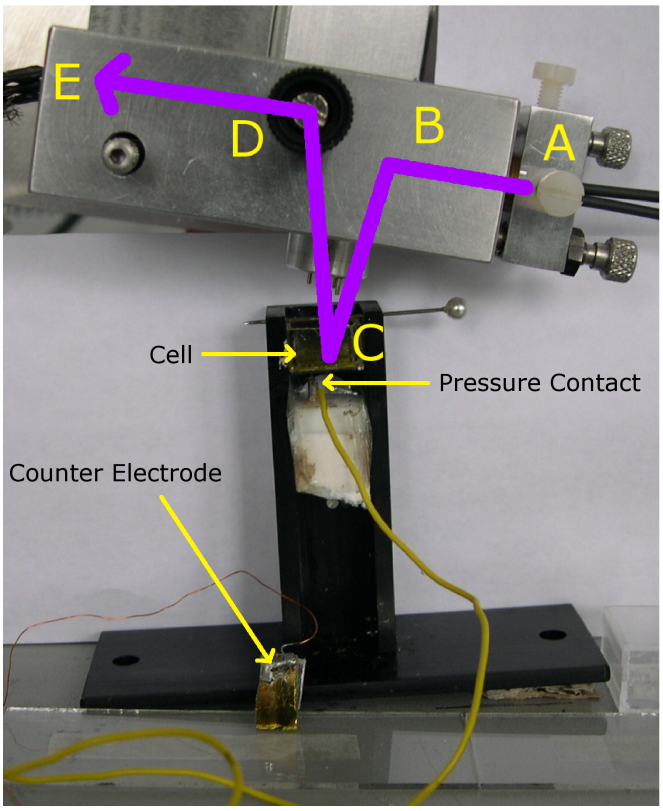

Figure 7.2. Components: LED (A), mirror (B), cell (C), rotatable mirror (D), quadrant diode (E)

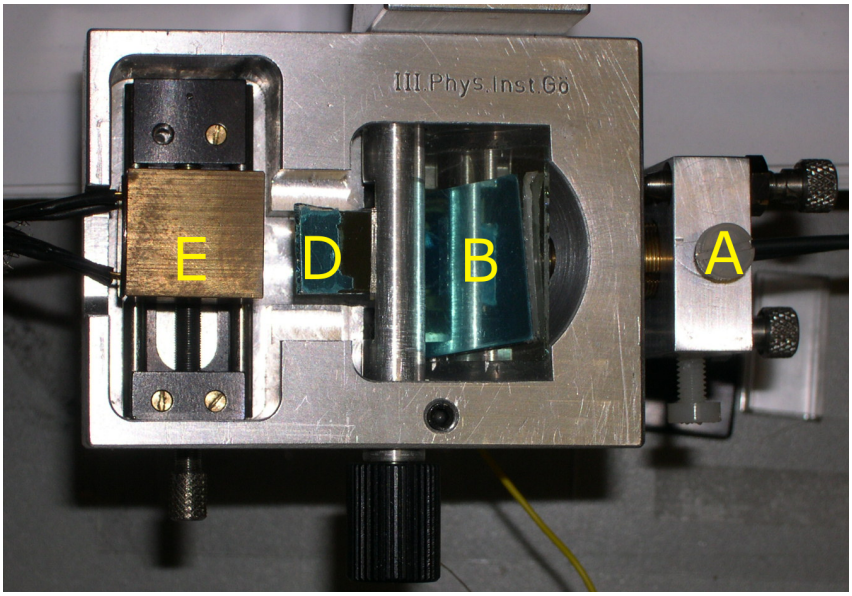

Figure 7.3.

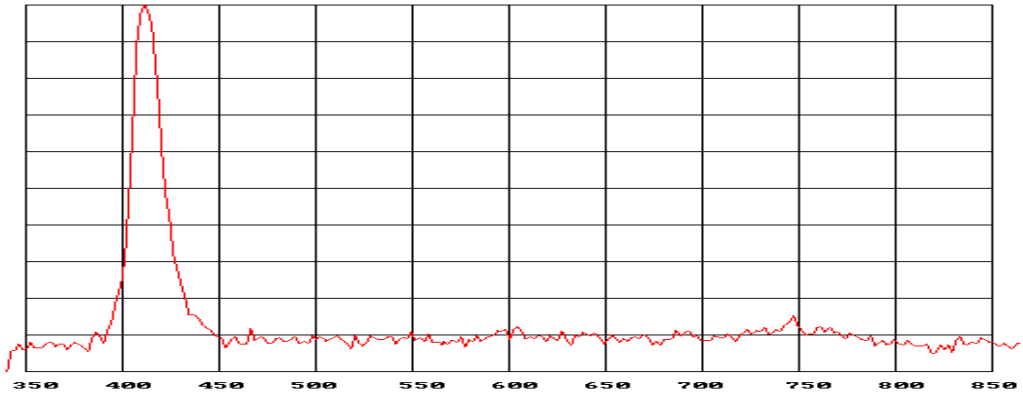

Figure 7.4. Typical emission spectrum of a purple LED [29].

7.2 Construction of the Cell

Two kinds of surfaces were used in the experiments. One was a silicon wafer with a 50 nm oxide layer. The other was a gold surface that was deposited on the silicon wafer by electron beam evaporation. This technique works by aiming a beam of accelerated electrons onto a target. As a consequence of the deposited energy some target atoms evaporate, which then condensate on the sample.

Initially the experiment was carried out with the silicon oxide wafers only, but since no effect was observed the gold coated surfaces were employed as well. The reason is that the gold surface provides a clearly defined surface potential, whereas in the case of the silicon wafer various layers of contacts and insulators make it more difficult to estimate the actual surface potential.

As depicted in Fig. 7.5 the silicon wafer was cut into square pieces with dimensions of 12 mm $\times$ 12 mm in order to fit onto the top of a cuvette that is used for regular photometric assays. Prior to glueing the cuvette onto the wafer it was cut to a length of 7 mm. The electrical contact was established by applying an gallium aluminium eutectic to the bottom side. To verify the quality of the contact, the eutectic was applied on two not connected spots, which allowed the measurement of the electric resistance between them.

In the case of the gold coated wafer the electric contact was made by using a conductive silver paint that was applied to one rim and the bottom of the wafer prior to glueing the cuvette onto it. Details of the complete preparation procedures are found in Appendix B.

The described method of measuring the absorption through the entire substrate solution volume requires that the functionalized surfaces have a sufficiently high reflectivity. In the case of gold this prerequisite is easily fulfilled but also the silicon surface exhibits a sufficiently strong reflectivity.

The counter electrode was made of a smaller piece of wafer with a 100 nm gold film on its surface. Electrical contact was established by simply soldering a thin copper wire onto it.

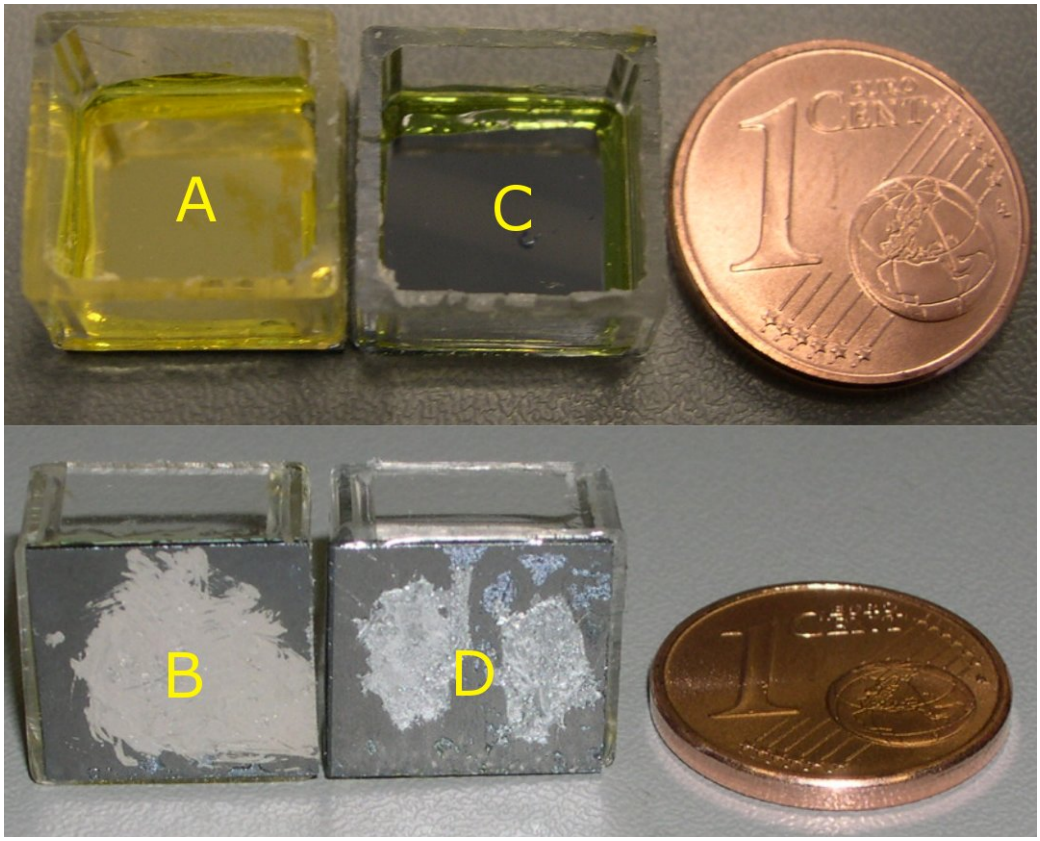

Figure 7.5. Images of the measurement cells: the gold coated cell (A,B) and the SiO_2 cell (C,D). Electrical contact to the sample is made by conductive silver paint in the case of the gold cell (B) and with a gallium aluminium eutectic in the case of the silicon wafer (D).

7.3 The Substrate pNPP

In order to spectrometrically observe and quantify the activity of the alkaline phosphatase, the substrate p-nitrophenyl-phosphate (pNPP) was employed. Alkaline phosphatase catalyzes the hydrolysis of pNPP, yielding the reaction products p-nitrophenol and a phosphate ion (Fig. 7.6 A). Before the spectrometric detection of the reaction product is possible, the p-nitrophenol has to undergo a further reaction with a hydroxide ion which removes the proton from the phenol, thus causing a strong absorption of light at a wavelength of 405 nm (Fig. 7.6 B).

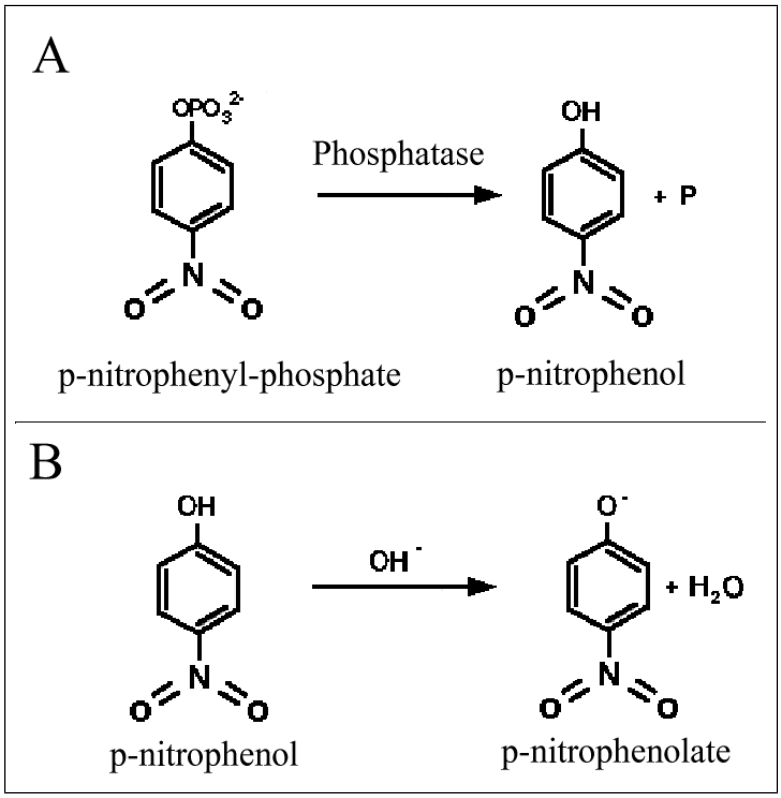

Figure 7.6. Reaction scheme of the pNPP substrate.

7.4 Quantification of Phosphatase Activity

The catalytic activity of the immobilized phosphatase was determined in a standard photometric assay with a fully populated wafer. The sample was immersed in a solution containing 2.7 mM pNPP, 40 mM TRIS buffer and 1 mM $MgCl_2$. The absorption was measured at a wavelength of 405 nm with a spectrometer UV-2102PC from Shimadzu Scientific Instruments. The turnover rate was determined to be 3200 s^{-1} at a temperature of 22 °C. This is a reasonable value when compared to the manufacturer supplied value of 4200 s^{-1}, which was measured at 37 °C in solution.

7.5 Immobilization on Gold

Since sulfur organic groups, such as thiols and disulfides, can bind tightly to gold surfaces they are often utilized for the formation of self-assembled monolayers (SAM) [30]. Functionalized gold surfaces are frequently employed in biosensor applications that involve the measurement of electrical characteristics such as conductivity or capacitance upon adsorption of a specimen [31].

As for the biotinylization of the SiO_2 surface, the modification of gold is also a multi step method. In the first step the surface is exposed to 16-Mercaptohexadecacanoic acid (MHA), which is a commonly used thiol for the formation of SAMs gold. Next, the now displayed carboxylic acid (COOH) groups are activated by reaction with N-hydroxysuccinimide and 1-(3-dimethylamino)propyl-N-ethyl-carbodiimide. The activated groups are then ready to bind biotinyl-3-6,9-trioxaundecanediamine in order to provide the biotinylization. A detailed protocol is given in Appendix B.

For compatibility with the experimental setup the gold was deposited on the same square pieces of silicon wafer that were used otherwise. Figure 7.7 shows an AFM image of a 100 nm gold film which was deposited by electron beam evaporation on the silicon wafer. The coarse structure is typical for vapor deposited metal films.

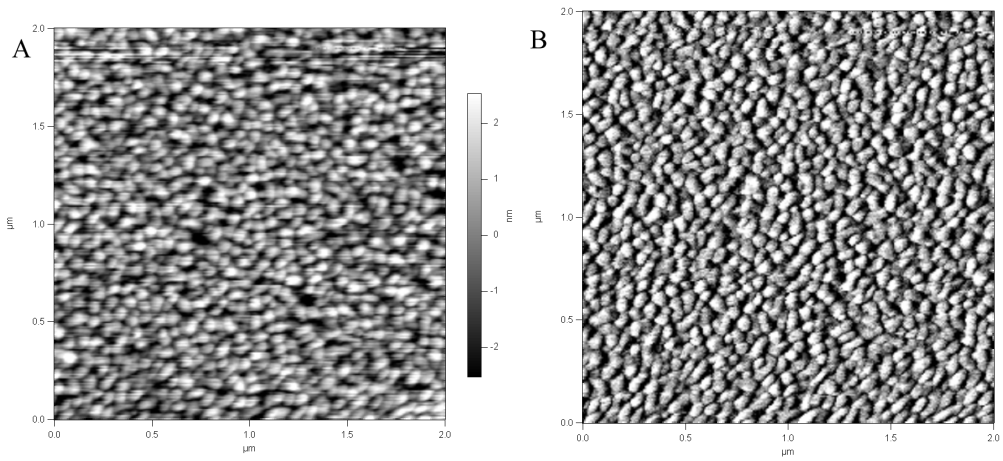

Figure 7.7. Height (A) and deflection (B) AFM images of a 100 nm gold film, which was deposited by electron beam evaporation.

7.6 Immobilization on SiO_2

The preparation of the functionalized silicon oxide surfaces follows mainly the protocol given in section 4.2. The difference is that the concentration of the protein solution has to be at least 100 nM in order to provide a surface that is completely covered.

7.7 Experiments

Usually an experiment took 1000-2000 s (15-30 min) and the surface potential was adjusted every 100-200 s in order to observe changes in the absorption curve that would be due to a changed protein activity. A typical time curve for a gold surface is shown in Figure 7.8, in which each color change indicates a change of the applied electrical potential. To be able to distinguish the change of the slope that is due to the consumption of the substrate from the anticipated regulative effect, the electric potential was alternated between 0 V and the respective applied voltage. The largest potential that was applied was 1 V in order to stay below the dissociation voltage of the water. The polarity was chosen according to the direction of the intended pH shift.

The first experiments were carried out with substrate solutions containing 1 mM pNPP, 1 mM TRIS buffer and 1 mM $MgCl_2$. The pH was adjusted to a value of pH 9.8, which is the optimum value for the alkaline phosphatase activity as seen from Figure 6.2. The idea was to shift the pH away from this optimum by applying the electric potential to surface.

Since neither the SiO_2 surface nor the gold surface exhibited any measurable effect, it was suspected that the TRIS buffer inhibits the change of the pH. Moreover, the bivalent magnesium ions contribute to a strong screening of the surface potential. Both potential obstacles let to the decision to remove the two compounds from the substrate solution.

It turned out that the plain substrate solution, adjusted to pH 9.8, still did not show any effect. To reduce the buffer capacity of the substrate, its concentration was lowered 0.1 mM but still no improvement was observed.

It was also attempted to start with a too low pH and to then shift the pH towards higher values to promote the protein activity. For this, the substrate was dissolved in plain deionized water. Again, this was to no avail.

7.8 Results

From Figure 7.8 it becomes apparent that no change of the slope between the alternating potentials is detectable that would indicate a change in the protein activity. For none of the varying experimental condition such an observation was made.

The relatively large width of the curve originates from the fact that the surface of the substrate solution is constantly oscillating due to external vibrations. Zooming into the plot reveals this periodic oscillation. Because of the relatively high sample rate of 10 Hz this effect can be easily averaged out.

Another systematic error stems from the evaporation of the substrate solution. Since the curved surface acts like a lens, small changes of this curvature that are caused by the evaporation, show up in the intensity signal as a constant slope. This effect could be minimized by providing a water saturated atmosphere. This was accomplished by carrying out the experiments under a cardbox whose inner sides had been equipped with humidified fabric.

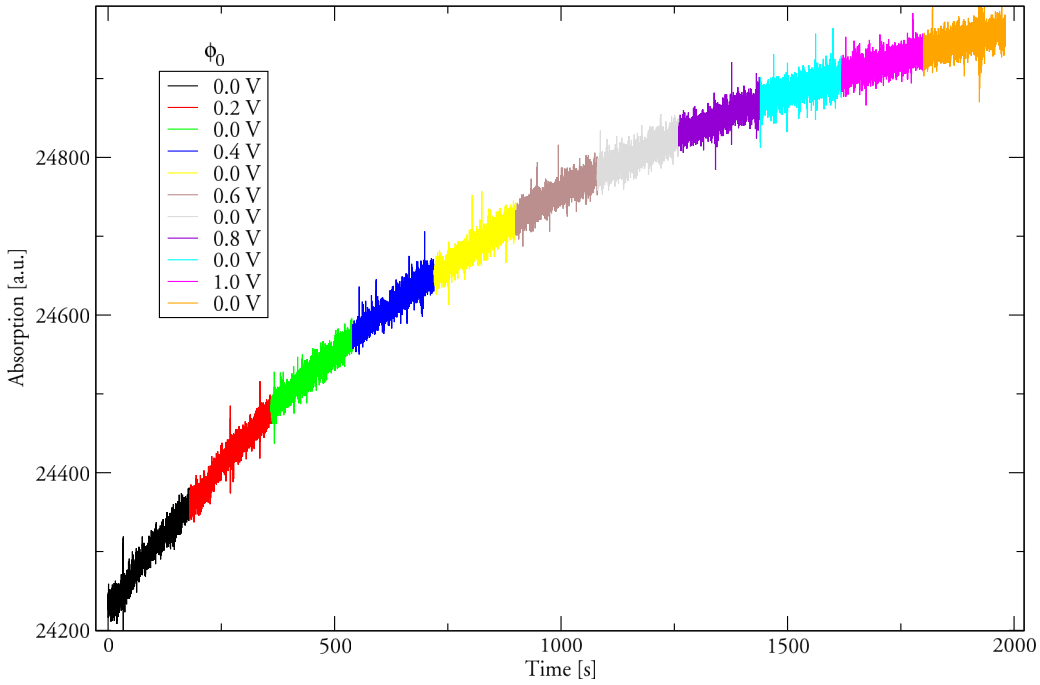

Figure 7.8. Typical time curve of an experiment. The color changes of the curve indicate a change of the surface potential.

7.9 Discussion

Recalling the theoretical background provided in section 6.2, possible arguments can be made out that help to explain the experienced failure. Considering the physical dimensions of molecules that are involved in the attachment of the phosphatase, namely the silane, the NHS-biotin and the streptavidin, it is fair to assume that the active site of the phosphatase is found at a distance around 10 nm from the surface.

From Figure 6.7 we find that in the case of a 1mM monovalent ionic solution the inducible pH shift at a distance of 10 nm is only in the order of 0.5-1 pH units. This helps to explain the failure in the case of the experiments that had a high buffer and substrate concentration.

But even in the experiments that were carried out only in the presents of deionized water and a very low substrate concentration, no effect was observed although the inducible pH shifts are estimated to be in the order of 3-4 pH units as suggested by Figure 6.5. Eventually, the screening of the electric potential is still too significant, even at a 0.1 mM substrate concentration.

Another important consideration might be the buffer capacity of the proteins and the substrate itself as discussed in section 6.5. Small changes of the pH that might be induced by the surface potential could get buffered by these compounds, thus covering up any significant effect.

The next section will discuss an alternative experiment, that avoids many of the afore mentioned potential problems.

7.10 Optical pH Measurement

In order to rule out the possibility that the spectrophotometric experiment is faulty and not able to detect any influence of the surface potential on the protein activity, it would be favorable to design an alternative experiment in which the measurement of the pH is based on a different principle.

The idea is to take advantage of the pH dependence of certain fluorophoric dyes. If brought into the vicinity of the charged surface it should be possible to observe a change in characteristics of the emitted spectrum. A prominent representative of pH dependent fluorophores is *fluorescein*. This substance exhibits multiple, pH dependent ionic equilibria which result in a variation of the intensity of the emitted light. Figure 7.9 depicts these different ionic states of fluorescein and Fig. 7.10 displays the pH dependent emission intensity.

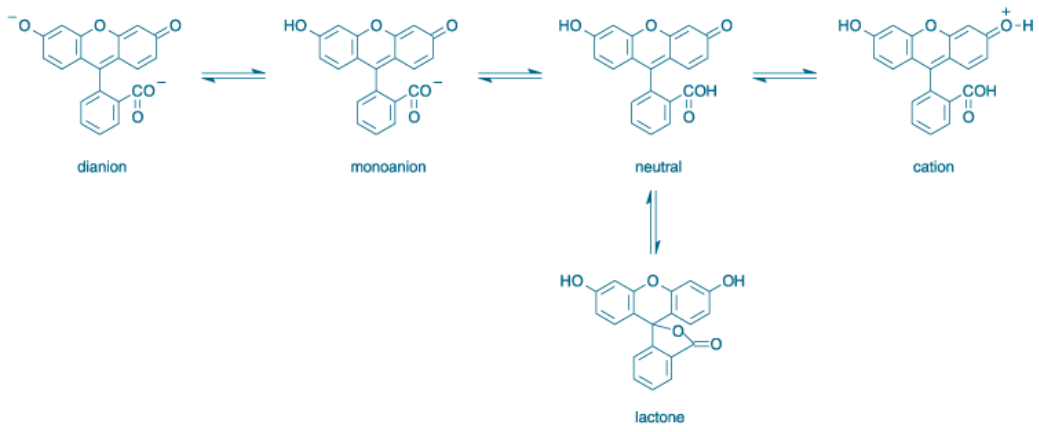

Figure 7.9. Different pH dependent ionic equilibria of fluorescein. Taken from [32].

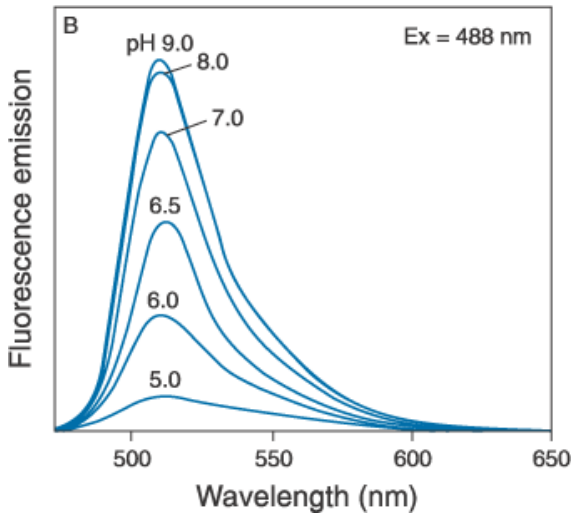

Figure 7.10. The pH dependent emission intensity of fluorescein. Taken from [32].

Fluorescein is available as many different conjugates. For this experiment most useful are the streptavidin-conjugated fluorescein and the NHS (N-hydroxysuccinimide-ester)-conjugated fluorescein. Both components can be immobilized on the silicon oxide wafer by the strategies described in section 4.2.

What makes the NHS-fluorescein very interesting is the fact that it can be bound *directly* to the amino groups of the EDA silane. This allows to abandon the streptavidin which brings the fluorophore much closer to the surface, thus increasing the effect of the applied electric potential. Another big advantage stems from the fact that no protein is present whose buffer capacity could come into play.

The experiment requires the modification of a regular spectrophotometer that is capable of detecting fluorescence. By mounting the functionalized surface in such a way that it is exposed to the excitation light and at the same time visible to the detection unit, the fluorescence should be observable.

A systematic approach to measure the pH dependent effects with this method would be to study:

- the pH dependence of plain fluorescein in solution
- the pH dependence of NHS-fluorescein in solution
- the pH dependence of NHS-fluorescein immobilized on glass
- the pH dependence of NHS-fluorescein immobilized on silicon oxide wafer

---

- the pH dependence of streptavidin-fluorescein in solution
- the pH dependence of streptavidin-fluorescein immobilized on glass
- the pH dependence of streptavidin-fluorescein immobilized on silicon oxide wafer

---

- application of electric potentials to NHS-fluorescein immobilized on silicon oxide wafer
- application of electric potentials to streptavidin-fluorescein immobilized on silicon oxide wafer

By using the NHS-fluorescein, which binds directly to the silane, the influence of the buffering effect of proteins or the substrate can be avoided. Moreover it is possible to bring the pH sensitive moiety closer to the electrically charged surface, which makes the observation of the anticipated effect more likely.
This experiment might be able to answer the questions for the failure of the photometric experiment.

Part III

The Self-Built AFM

8

The Self-Built AFM

Real programmers don't comment their code.
It was hard to write, it should be hard to understand.

Anonymous

8.1 Introduction

In the early course of this work, when the idea of producing nanolithographic patterns was developed, there was no AFM available within the research group that would have been applicable to the task. In order to attain the required flexibility for doing nanolithography it was decided to build an AFM on our own.

The big advantage of this approach was that the instrument could be designed with a specific application in mind. Since for example this AFM was only to be used in experiments involving molecules, the scan range of the piezo stage could be comparatively small as opposed to the experiments where larger samples, such as cells, are of interest. A small scan range of the piezo stage leads to small physical dimension of the piezo, which in turn allows for high scan speeds. The idea of keeping the mechanical parts small and compact is a major precept of AFM design, because in such a design the mechanical resonance frequencies are higher than the frequencies that are relevant for the imaging process.

Another important design decision was to be able to use the fluid-cell/cantilever-holder from a commercial instrument (Veeco Nanoscope IIIa). The reason for this is that due to the required transparency this compound is made of glass, which makes it difficult to fabricate.

The laser for measuring the deflection and torsion of the cantilever was chosen to operate in the infrared regime because of the stability of the beam and the unique property of being fairly decoherent, which has the advantage of reducing the effects of interference.

8.2 Hardware

8.2.1 Mechanical Hardware

The mechanical design can basically be separated into the *stage* and the *head* of the AFM. The stage contains essentially the piezo for the XYZ-positioning of the sample as well as three leveling screws. These screws support the head and allow for precise adjustment of leveling and height. Figure 8.2 shows an image of the stage.

The piezo is a commercial product (P-363, Physikinstrumente GmbH, Germany) and is unique in the sense that it has a very compact design with a scan range of 6 µm for each axis. It also features a capacitive feedback, which measures the current position of the piezo and compensates for non-linearities in the movement. This feature allows the extraction of the Z-position of the piezo, respectively the height of the sample. Additionally the information about the XY-position can be used to evaluate the quality of the scanning at high scan speeds. The piezo is connected to a unit that contains the electronics for the capacitive feedback and the high voltage generators. The connectors of the unit allow the feeding of the XYZ-positioning signals from a computer and the readout of the XYZ-positions measured by the capacitive distance sensors.

The head can be distinguished into several parts as well. For one there is the mounting of the laser, which is constructed as an adjustable tripod to allow the positioning of the focused laser onto the cantilever. Then there is the lever for holding the fluid-cell in place. Its pressure contacts allow for an electrical connection to the driving piezo inside the fluid-cell when operating in tapping mode. Once the laser is reflected from the cantilever it falls onto a mirror, which can be rotated along one axis. The reflected beam than hits the quadrant diode, which can be positioned with a XY-translation unit in order to center the laser spot. An image of the head is found in Fig. 8.4.

8.2.2 Electrical Hardware

Before the signal from the quadrant diode can be sampled by the data acquisition boards, it first has to undergo some analog processing, which is depicted in Fig. 8.1.

At first the weak signals from each quadrant get enhanced by a low noise operation amplifier. The amplifier is located close to the quadrant diode inside the AFM head. For details of the circuit layout the reader is referred to Appendix C, Fig. C.4.

In the next processing stage the sum of all quadrants, the vertical and the horizontal deflection are determined from the amplified signals. The required calculations are also carried out with a set of operation amplifiers. For details on the actual implementation see Appendix C, Fig. C.2.

Depending on the mode of operation (Contact/Tapping) either the deflection or the amplitude of the cantilever oscillation is of interest. In order to determine the amplitude of the oscillation the signal is processed in a so called *absolute value circuit*. In this circuit the AC part of the deflection signal is first decoupled from the DC part

and then rectified. After low-pass filtering the amplitude is obtained. For details the reader is referred to Appendix C, Fig. C.1.

The forwarding of either deflection or amplitude to the data acquisition board is done via TTL signals that cause a multiplexer to select the one or the other. Details are found in Appendix C, Fig. C.3.

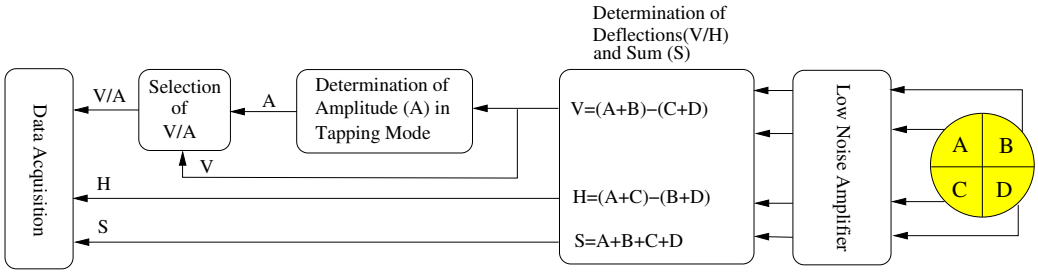

Figure 8.1. Schematics of the analog signal path.

Except for the low noise amplifier all afore mentioned circuits are build on two bread-boards which are housed in a 19" slide-in unit.

After the pre-processing the signals are ready to be sampled by the data acquisition (DAQ) boards, which are two PCI cards (PCI-6052E, National Instruments) that are installed in a regular dual processor PC (2x Pentium III, 1.4 GHz). These boards offer a sample rate of 333 kS/s at a resolution of 16-Bit. Additionally, each of them offer two 16-Bit analog outputs.

8.3 Software

In order to have maximum control over all aspects of the instrument and for the sake of stability, the entire software is based on *Open Source* components. For a more detailed description of what Open Source is and which components were employed, the reader is referred to Appendix D.

The description of the software is distinguished into two parts: One that deals with the realtime part describing all aspects of data acquisition and realtime processing and the other, which describes the user interface and scripting capabilities.

8.3.1 Realtime Part

Operating an AFM is a highly dynamic process which requires strict control over the positioning of the AFM tip and the data acquisition. The approach of a new spot on the scanning raster, for example, has to be synchronized with the sampling of the corresponding deflection. Even higher demands are required by the feedback loop which takes care of the dynamic positioning of the sample in the Z direction. An operating system that is able to provide such strict timing demands is called a *realtime* operating system.

To provide these realtime requirements many commercial AFM manufacturers use dedicated processors (DSP, FPGA). Since these devices are committed to the realtime tasks, no special measures have to be taken to fulfill the rigorous timing demands. The disadvantage is that these processors often require proprietary programming tools and means of communication to connect to a host PC to control the unit.

In the case of the self-built AFM, it was decided to avoid the approach with a dedicated real time unit, but rather employ a generic operating system with realtime capabilities and also to use generic data acquisition boards which connect to the PCI bus. The advantage of having the realtime components (software and hardware) merged with a regular workstation is that the PC is at the same time available for the visualization and analysis of the acquired data. Since everything is in "one box", the communication between the different components can be efficiently implemented.

The realtime operating system used for the self-build instrument is LINUX with a modified kernel. These modifications are developed by the RTAI project (Appendix D) and give the kernel hard realtime capabilities with an interrupt latency of less than 10 µs. While not committed to any realtime task, the non-realtime part of the system is available for any other task such as visualization or user interaction. Due to the tight binding to the kernel and the need for fast reaction times, the realtime modules are implemented in plain C.

The communication with the data acquisition boards takes place via the *Comedi* library (Appendix D). Among many other features, this software component allows to issue simple commands such as reading or writing voltages to the DAQ boards in the realtime context. In order to efficiently distribute the necessary tasks, one of the DAQ boards is assigned to any task that deals with controlling the piezo stage in XY direction, whereas the other deals explicitly with controlling the Z direction, in particular the feedback loop.

8.3.2 User Interface Part

The graphical user interface (GUI) is responsible for the visualization of the acquired data and the processing of user inputs, such as zooming into a selected area or analyzing an acquired image. As opposed to the realtime component the GUI is not implemented in C but rather in Python, a high level object orientated language. Python provides binding to a rich set of libraries for all kinds of applications. For example the standard GUI components like menus and buttons are based on *Qt*, whereas the plotting of 2D graphs is based on *PyQwt*, just to mention a few. The advantage of using Python is that the GUI can easily be modified and extended to fulfill new demands. Again, for a more detailed list of the software components employed see Appendix D.

On the application programming interface (API) side, the user can access all important realtime functions, such as acquiring a force-curve or just moving to a specific position, from regular python function calls. This allows the design of unique experiments by just writing simple python scripts.

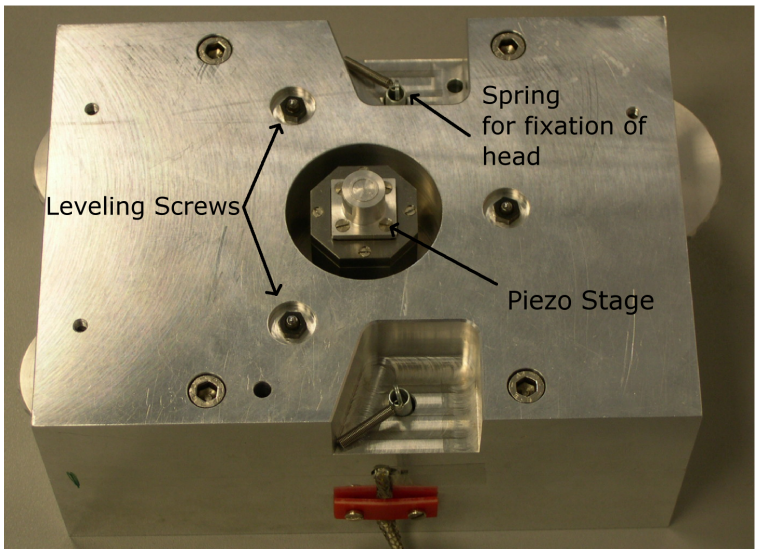

Figure 8.2. This image shows the AFM stage. The turning wheels on the edges adjust the leveling screws.

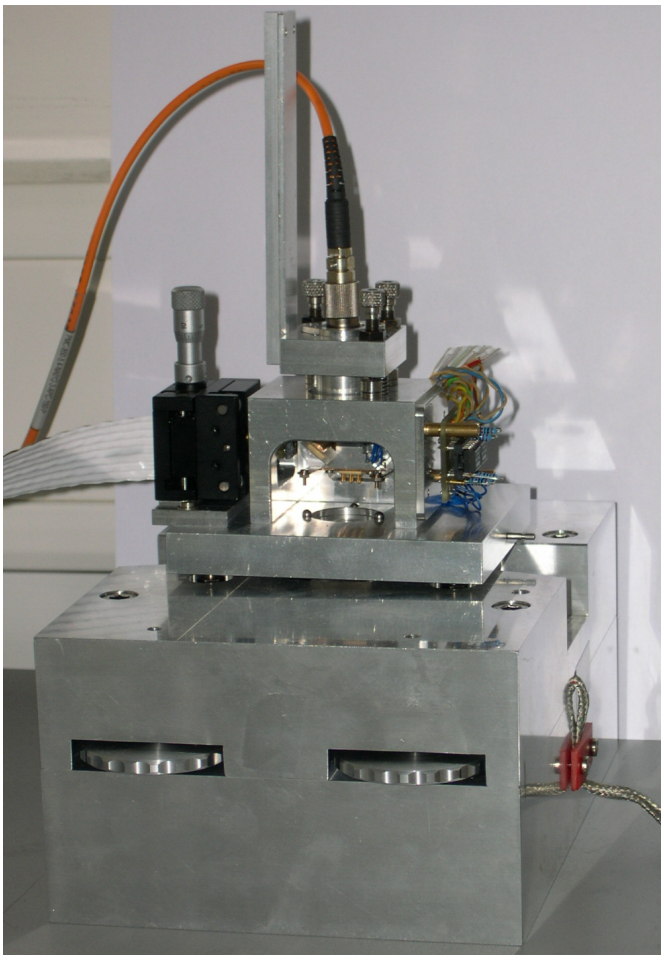

Figure 8.3. AFM head and stage combined to the functional unit.

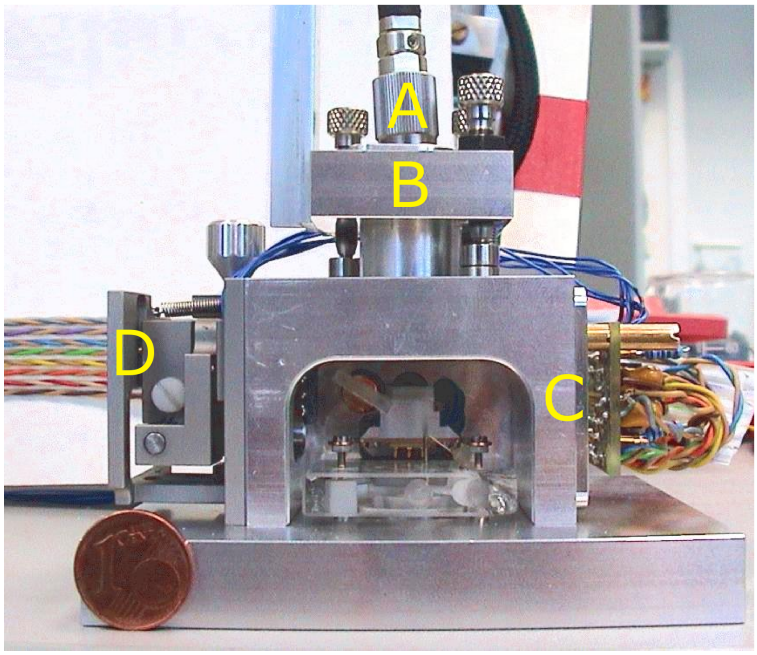

Figure 8.4. AFM head consisting of: laser (A), tripod (B), low noise amplifier (C) and XY-translation unit (D).

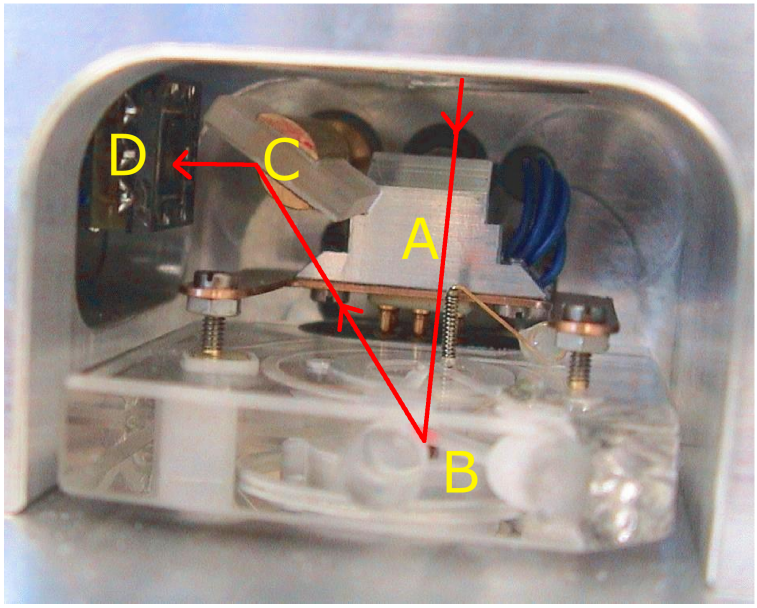

Figure 8.5. Close up of the AFM head showing the lever for fixation of the fluid cell, the fluid cell including chip mounting (B), the rotatable mirror (C) and the quadrant diode (D). The red line indicates the path of the laser beam.

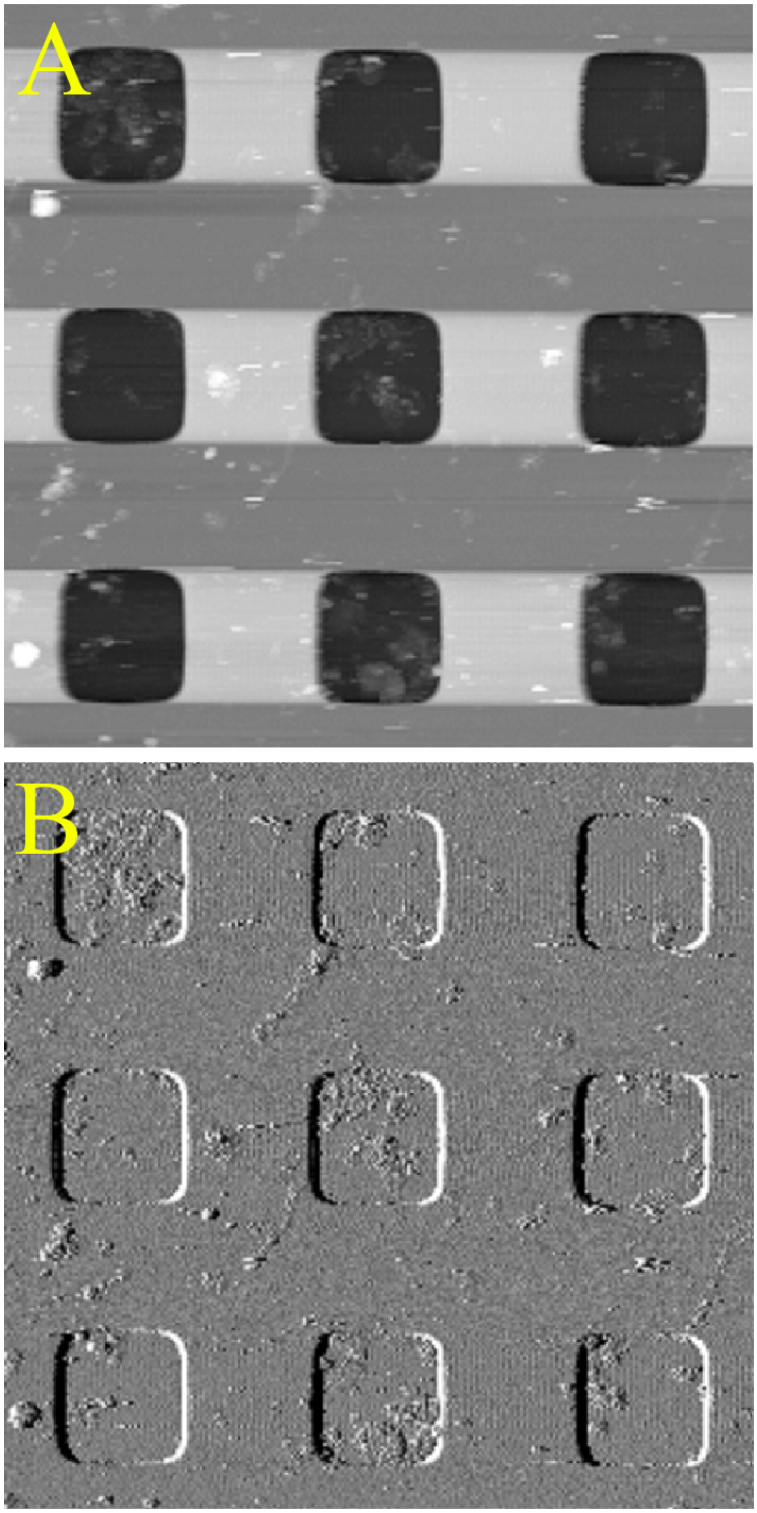

Figure 8.6. This figure shows the height (A) and deflection (B) image of a (admittedly dirty) calibration grid obtained by the self-build AFM. The pitch of the squares is 10 µm and the depth is 200 nm. This image was obtained with a prototype version of the AFM that had a large scan range, which allowed the imaging of this structure. The light horizontal stripes in the height image originate from the fact that each scan-line is line-fitted.

A

Chemicals

List of chemicals and suppliers:

Item	Supplier / Product No.
Methanol .p.A	Riedel de Haen - 32213
Sulfuric Acid p.A.	Riedel de Haen - C8029
Silicon Oxide Wafer	Crystec, Berlin S 3012
Deionized Water	Millipore GmbH, Eschborn
Acidic Acid conc. p.A.	Fluka 45731
Dimethyl Sulfoxid (DMSO) 99,9 %	Fluka 41640
N-2-aminoethyl-3-aminopropyltrimethoxy-silane	Merck 8.19172.0100
Biotin-N-hydroxysuccinimid-ester (NHS-Biotin)	Sigma H1759
Ethanol p.A.	Riedel de Haen 32205
p-nitrophenyl-phosphate (pNPP)	Sigma N4665
TRIS buffer p.A.	Roth 4855.2
Magnesiumchloride 99 %	Sigma M2670
Alkaline phosphatase – Streptavidin conjugated	Sigma S-2890
16-Mercaptohexadecacanoic acid 90 %	Aldrich 448303-1G
Biotinyl-3-6,9-trioxaundecanediamine	Pierce 21347
N-hydroxysuccinimide (NHS)	Fluka 56480
1-(3-Dimethylamino)propyl-N-ethylcarbodiimide	Aldrich 16.146-2
BCIP/NBT	Sigma B-6404
(3-Glycidyloxypropyl)trimethoxy-silane	Sigma G-1535
Silver conductive paint	RS Components 186-3593
5-min Epoxy Glue	Bindulin Werke, Germany

B

Preparation Protocols

Deposition of Gold on Wafer

- Immersion of square pieces of SiO_2 wafer (12 mm $\times$12 mm) in a mixture of concentrated sulfuric acid and hydrogen peroxide (3:1) in a sonicator for 15 min
- Rinsing with deionized water
- Drying in stream of nitrogen
- Application of 5 nm platinum as an adhesion layer by electron beam evaporation
- Application of 100 nm gold by electron beam evaporation
- Storing the samples under vacuum

Biotinylization of Gold

- Preparation of saturated solution of 16-mercaptohexadecacanoic acid (MHA) in methanol by sonication for 5 min
- Immersion of gold coated piece of wafer in MHA solution for 12h
- Rinsing two times with methanol
- Drying in stream of nitrogen
- Activation of COOH groups by immersion of sample in solution of 0.2 M M-hydroxysuccinimide (NHS) and 0.1 M 1-(3-dimethylamino)propyl-N-ethylcarbodiimide (EDAC) in deionized water for 30 min.

- Rinsing two times with ethanol
- Rinsing with deionized water
- Drying in stream of nitrogen
- Application of 150 µl of 10 mM solution of Biotinyl-3-6,9-trioxaundecanediamine (Biotin-NHS) in deionized water onto the sample
- Rinsing with deionized water
- Drying in stream of nitrogen

This procedure is based on [20]

Biotinylization of SiO_2

Cleaning

- Immersion of the sample in a mixture of concentrated sulfuric acid and hydrogen peroxide (3:1) in a sonicator for 15 min
- Rinsing with deionized water

Silanization

- Preparation of a solution containing:

  - 9 ml Methanol
  - 80 µl Acetic acid
  - 370 µl Deionized water
  - 230 µl N-2-aminoethyl-3-aminopropyltrimethoxy-silane

- Immersing the sample in this solution for 30 min
- Rinsing the sample two times with methanol
- Drying in a stream of nitrogen
- Curing the sample for 3 min at 120 °C

Attachment of the biotin linker

- Preparation of a solution containing:

  - 4 ml dimethyl sulfoxide (DMSO)
  - 1 µg biotin-N-hydroxysuccinimide-ester (NHS-Biotin)

- Immersing the sample in this solution for 2h
- Rinsing the sample two times with ethanol
- Drying in a stream of nitrogen

This procedure is based on [19]

Application of Streptavidin-Conjugates

- Application of a 0.2 nM solution of streptavidin conjugated AP in buffer for 10 min results in a sparsely populated surface. For complete coverage the proteins concentration should be at least 100 nM
- Rinsing with deionized water
- Incubation in a 2.7 mM (1µg/ml) solution of p-nitrophenylphosphate (pNPP) in 40 mM TRIS buffer and 1 mM magnesiumchloride for 10 min on a stirrer in order to remove streptavidin-conjugates that are not tightly bound to the surface
- Rinsing with deionized water

Construction of SiO_2 Cell

- Sawing off the top 7 mm of a disposable cuvette (12mm × 12 mm)
- Preparation of 5-min epoxy glue on an object slide
- Dipping the flat side of the cuvette top in the glue and placing it centered on the biotinylated piece of wafer
- Blowing a stream of nitrogen on the biotinylated surface while the glue is curing
- Application of the streptavidin conjugate solution to the surface

Establishing electrical contact to the silicon wafer

- Wearing protective gloves is recommended
- Scraping the bottom side of the cell with a glass cutter
- Grinding a prolated aluminum stick in gallium in order to form an eutectic on the tip of the stick

- Application of the eutectic to scraped area of the cell on two not connected spots
- Measure the electrical resistance between the two spots. If not in the order of 1-200 Ω (depending on the doping of the wafer) repeat the scratching

Construction of Gold Cell

- Cutting of the top 7 mm of a disposable cuvette (12mm × 12 mm)
- Preparation of 5-min epoxy glue on an object slide
- Application of conductive silver paint to on edge of the gold coated wafer, so that the gold is connected. Painting the bottom side of the cell as well.
  Note: The thinner the layer is, the better it works!
- Dipping the flat side of the cuvette top in the glue and placing it centered on gold coated piece of wafer
- Blowing a stream of nitrogen on the biotinylated surface while the glue is curing
- Application of the streptavidin conjugate solution to the surface
- Verifying the electrical contact by measuring the electrical resistance between the bottom and the top side of the wafer

C

Electric Circuit Layouts

A) Determination of Amplitute in Tapping-Mode

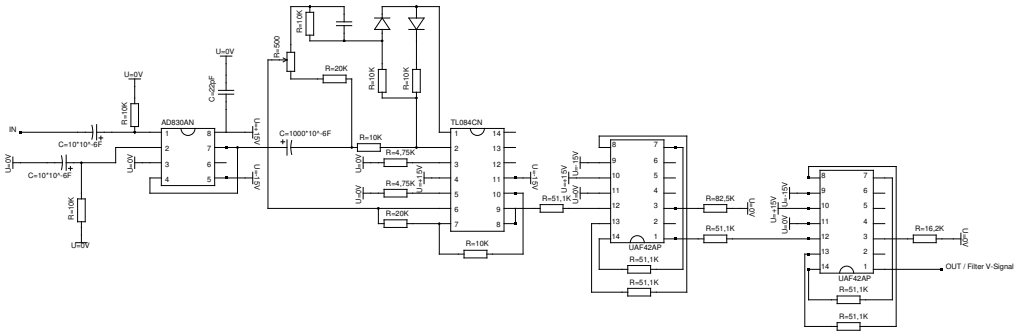

Figure C.1. In a first stage the AC part of the signal is decoupled from the DC part (AD83AN), which then is simply amplified by a operation amplifier (TL084CN). Subsequently the signal is low pass filtered in a two stage active filter unit based on the UAF42AP, a versatile state-variable filter which can be adjusted by only choosing proper external resistors. The design of this "Absolute Value Box" is a result of merging circuits of a tried circuit [33] and ideas from the book *The Art of Electronics* [34].

B) Determination of Sum and Defelctions

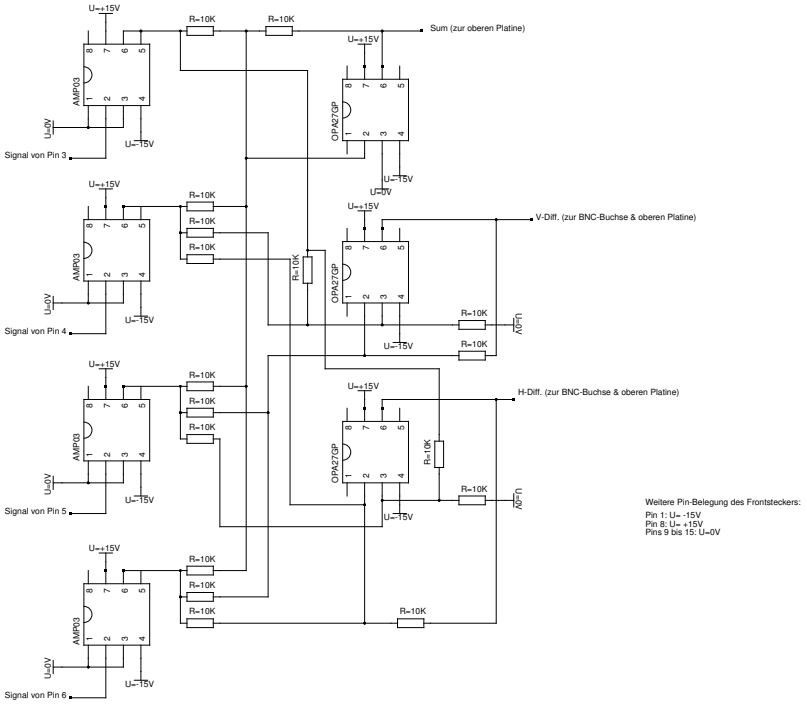

Figure C.2. This circuit calculates the sum, vertical and horizontal deflection depending on the inputs from each quadrant of the quadrant-diode. To accomplish this, the signals from the quadrants are each current-voltage converted using an operation amplifier AMP03. Then the appropriate signals are fed to a second stage where the required sums and difference are obtained from a set of OPA27GP operation amplifiers. The design is based on [33] .

C) Multiplexer to switch between Contact and Tapping Mode -> i)
and auxiliary multiplexer -> ii)

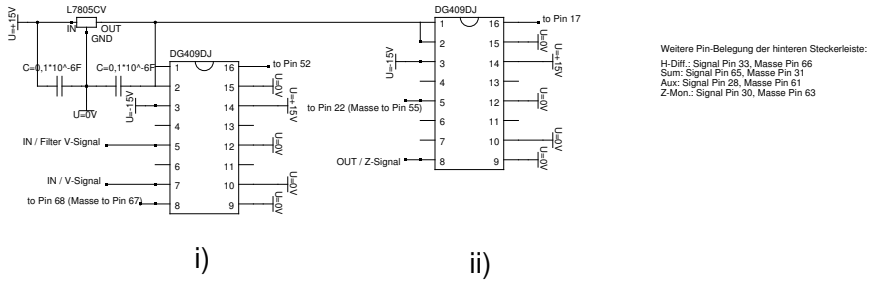

Figure C.3. This circuit shows the multiplexer (DG409DJ) that allow to select between two signals. Multiplexer i) selects between the deflection or amplitude depending on the TTL level on pin 8. The other unit is an auxiliary multiplexer for future use.

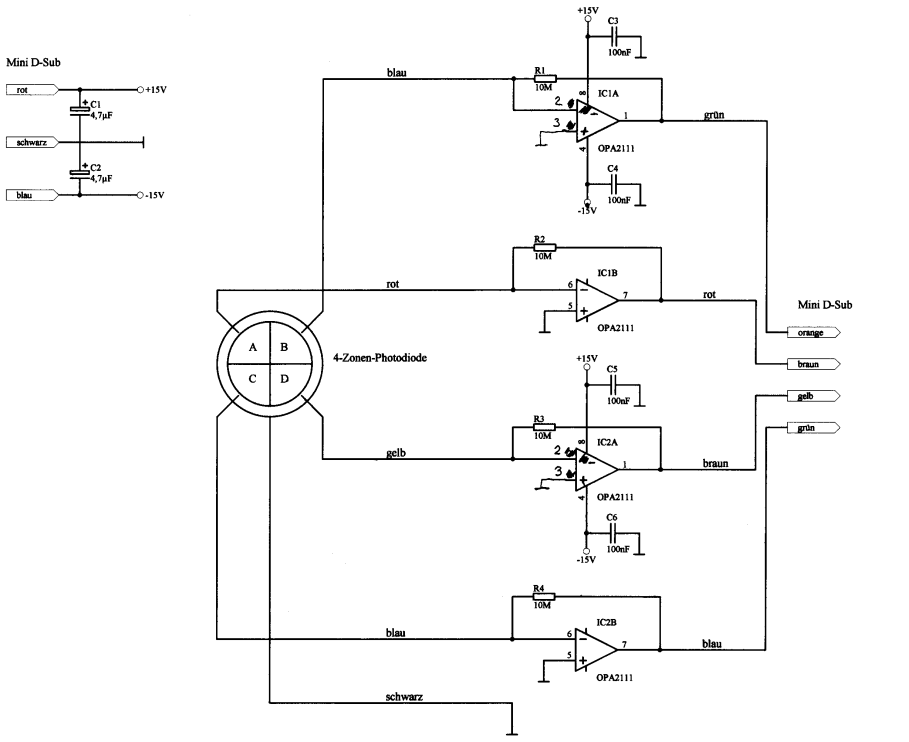

Figure C.4. This circuit shows the amplifier that enhances the voltages obtained from each quadrant of the quadrant diode. It is located very close to the detector and features an extremely low noise operation amplifier (OPA211). The design is based on [33] .

A Test for the Absolute Value Circuit

AFM cantilevers always experience a faint motion, due to thermal fluctuations they pick up from the surroundings. Depending on the force constant typical deflections are in the order of a few Ångstrom, which can be picked up by the detector. It is actually a good test for the low noise amplifier and the circuit for the analog calculation of the differences to detect this faint signal.

The idea was now to also verify the proper functioning of the circuit that determines the amplitude of the oscillation in tapping mode (Fig. C.1). This can be of course done by applying an external signal with a function generator, but the ultimate test would be to see if the electronics would be good enough to detect the amplitudes that are associated with the faint thermal motion.

Considering the thermal origin of this motion one would expect that the amplitude of the oscillation follows the Maxwell-Boltzmann distribution. The analogy is an ideal gas, in which the velocity of the particles display an analog behavior.

By sampling the amplitude of the deflection of the free cantilever for 5 s and calculating a histogram of the detected amplitudes, the anticipated behavior can be observed as depicted in Fig. C.5.

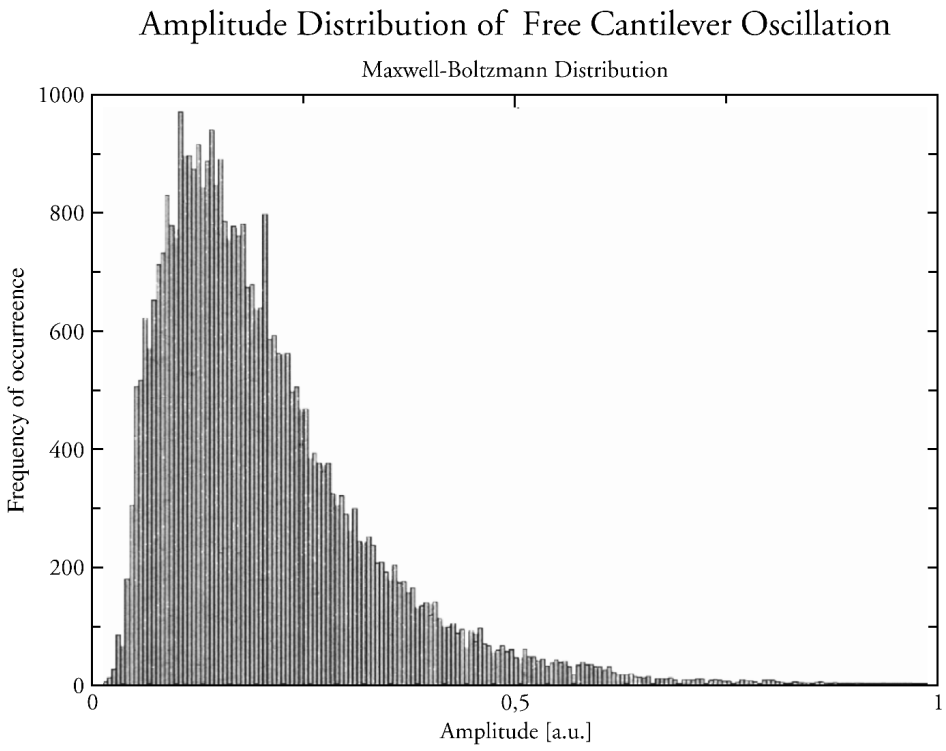

Figure C.5.

D

Software

The fast development of the self-built AFM would not have been possible without the broad software base that is provided by the Open Source community. To get an idea of the different software components that were employed, a list of quotations from websites that are related to the individual programs is provided.

- **Open Source** – http://www.opensource.org/

  The basic idea behind open source is very simple: When programmers can read, redistribute, and modify the source code for a piece of software, the software evolves. People improve it, people adapt it, people fix bugs.

- **Linux** – http://www.linuxlinks.com/local/WhatisLinux.shtml

  Linux is a complete operating system that is similar but not identical to UNIX. It runs on a wide variety of hardware, ranging from 386's/486's/Pentiums/Pentium II's to more exotic hardware such as Digital Alpha computers, PowerPCs, and Silicon Graphics workstations. Probably the most unique characteristic of Linux is that it is freely distributable. Freely distributable means that the source code for the kernel and most software cannot be withheld.

- **RTAI** – http://www.aero.polimi.it/ rtai/documentation/articles/guide.html

  RTAI is a modification to the regular LINUX kernel which enables it to provide *Real Time* functionality.

  What is a "real time system"?

  A real time system can be defined as a "system capable of guaranteeing timing requirements of the processes under its control".

It must be fast and predictable. Fast means that it has a low latency, i.e. it responds to external, asynchronous events in a short time. The lower the latency, the better the system will respond to events which require immediate attention. Predictable means that it is able to determine task's completion time with certainty.

What is RTAI?

RTAI means Real Time Application Interface. It is based on the Linux kernel, providing the ability to make it fully pre-emptable.

Linux is a standard time-sharing operating system which provides good average performance and highly sophisticated services. Like other OS, it offers to the applications at least the following services:

- hardware management layer dealing with event polling or processor/peripheral interrupts
- scheduler classes dealing with process activation, priorities, time slice
- communications means among applications.

Linux suffers from a lack of real time support. To obtain a timing correctness behavior, it is necessary to make some changes in the kernel sources, i.e. in the interrupt handling and scheduling policies. In this way, you can have a real time platform, with low latency and high predictability requirements, within full non real time Linux environment (access to TCP/IP, graphical display and windowing systems, file and data base systems, etc.).

- **Comedi** – http://www.comedi.org/

The Comedi project develops open-source drivers, tools, and libraries for data acquisition.

Comedi is a collection of drivers for a variety of common data acquisition plug-in boards. The drivers are implemented as a core Linux kernel module providing common functionality and individual low-level driver modules.

Comedilib is a user-space library that provides a developer-friendly interface to Comedi devices. Included in the Comedilib distribution is documentation, configuration and calibration utilities, and demonstration programs.

Kcomedilib is a Linux kernel module (distributed with Comedi) that provides the same interface as Comedilib in kernel space, suitable for real-time tasks. It is effectively a "kernel library" for using Comedi from real-time tasks.

- **Python** – http://www.python.org/doc/Summary.html

  What is Python?

  Python is an interpreted, interactive, object-oriented programming language. It is often compared to Tcl, Perl, Scheme or Java. Python combines remarkable power with very clear syntax. It has modules, classes, exceptions, very high level dynamic data types, and dynamic typing. There are interfaces to many system calls and libraries, as well as to various windowing systems (X11, Motif, Tk, Mac, MFC). New built-in modules are easily written in C or C++. Python is also usable as an extension language for applications that need a programmable interface.

- **Qt** – http://www.trolltech.com/products/qt/index.html

  Qt is a complete C++ application development framework. It includes a class library and tools for cross-platform development and internationalization. Qt applications run natively, compiled from the same source code, on all supported platforms.

- **PyQt** – http://www.riverbankcomputing.co.uk/pyqt/

  PyQt is a set of Python bindings for the Qt toolkit. The bindings are implemented as a set of Python modules: qt, qtcanvas, qtgl, qtnetwork, qtsql, qttable, qtui and qtxml, and contains 300 classes and over 5,750 functions and methods.

- **PyDVT** – http://www.esrf.fr/computing/bliss/python/PyDVT/

  PyDVT is a Python toolkit for data displaying developed at the ESRF by Alexandre Gobbo. PyDVT is multi-platform (Windows, Solaris, Linux and Hp) and GUI toolkit independent (is has already bindings to PyQt and Tkinter). It defines a framework for interconnecting generic data retrieving, processing, and displaying objects. The package includes implementation of standard displaying widgets (1d, 2d, mesh and contour plotting) and data retrieving classes to address most ESRF standard data sources. PyDVT classes can be extended to add custom functionality (new visualization widgets, data sources and operations).

- **QwtPlot** – http://qwt.sourceforge.net/

  The Qwt library contains GUI Components and utility classes which are primarily useful for programs with a technical background. Beside a 2D plot widget it provides scales, sliders, dials, compasses, thermometers, wheels and knobs to control or display values, arrays, or ranges of type double.

- **gsl** – http://www.gnu.org/software/gsl/

  The GNU Scientific Library (GSL) is a numerical library for C and C++ programmers. It is free software under the GNU General Public License. The library provides a wide range of mathematical routines such as random number generators, special functions and least-squares fitting. There are over 1000 functions in total.

Bibliography

[1] T. Rueckes et al. Carbon nanotube based nonvolatile random access memory for molecular computing. *Science*, 289(7):94, 2000.

[2] T.J. Reece et al. Nonvolatile memory element based on a ferroelectric polymer langmuir blodgett film. *Applied Physics Letters*, 82(1):503, 2003.

[3] K. Sakamoto et al. Molecular computation by dna hairpin formation. *Science*, 288(5469):1223, 2000.

[4] C. Brittain et al. Soft lithography and microfabrication. *Physics World*, 11:31, 1998.

[5] R.D. Piner et al. "dip-pen" nanolithography. *Science*, 283:661, 1999.

[6] R. Ionescu et al. Nanolithography using protease etching of protein surfaces. *Nanoletters*, 3:1639, 2003.

[7] Binnig at al. Atomic force microscope. *Phys. Rev. Lett.*, 56, 1986.

[8] Veeco Instruments: www.veeco.com.

[9] C.A.J. Putman et al. Tapping mode atomic force microscopy in liquid. *Appl. Phys. Lett.*, 64:2454, 2003.

[10] H.G. Hansma et al. Biomolecular imaging with the atomic force microscope. *Annu. Rev. Biophys. Chem.*, 23:115, 1994.

[11] P.C. Lyu: http://life.nthu.edu.tw/lslpc/StrucBio/folding/Folding_1.html.

[12] McComb et al. *Alkaline Phosphatase*. Plenum Press, New York, USA, 1979.

[13] E. E. Kim and H.W. Wyckoff. Reaction mechanism of alkaline phosphatase based on crystal structures. two-metal ion catalysis. *J Mol Biol*, 218:449, 1991.

[14] E. Mornet et al. Structural evidence for a functional role of human tissue non-specific alkaline phosphatase in bone mineralisation. *J. Biol. Chem.*, 276:31171, 2001.

[15] Janeway et al. Magnesium in the active site of escherichia coli alkaline phosphatase is important for both structual stabilization and catalysis. *Biochemistry*, 32:1601, 1993.

[16] N. Green. The nature of the biotin-binding site. *Biochem J.*, 89, 1963.

[17] S. Freitag et al. Structural studies of the streptavidin binding loop. *Protein Science*, 6:1157, 1997.

[18] RCSB Protein Data Bank: http://www.rcsb.org/pdb.

[19] David R. Baselt et al. A high-sensitivity micromachined biosensor. *Proceedings of the IEEE*, 85(4):672, 1997.

[20] J. Hyung et al. Molecular recognition-mediated fabrication of protein nanostructures by dip-pen lithography. *Nano Letters*, 2(11):1203, 2002.

[21] U. König et al. Plasma modification of polytetrafluoroethylene for the immobilization of the fibrinolytic protein urokinase. *Surface and Coatings Technology*, 116-119:1011, 1999.

[22] R. Polzius et al. Optimization of biosensing using grating couplers: immobilization on tantalu oxide waveguides. *Biosensors & Bioelectronics*, 11(5):503, 1996.

[23] Sven Blank. *Direkte Beobachtung der enzymatischen Aktivität einzelner alkalischer Phosphatasemoleküle*. PhD thesis, University of Bremen, 2003.

[24] M.S. Blake et al. A rapid, sensitive method for detection of alkaline phosphatase-conjugated anti-antibody on western blots. *Anal. Biochem.*, 136:175, 1984.

[25] Gem & Mineral MinersInc: http://www.mineralminers.com/html/mcaminfo.htm.

[26] G. Gouy. *J. Phys.*, 9(4):457, 1910.

[27] O. Stern. *Z. Elektrochem*, 30:508, 1924.

[28] J. Gareth Morris. *A Biologist's Physical Chemistry*. Edward Arnold Limited, London, UK, 1974.

[29] The LED Museum: http://ledmuseum.home.att.net/ledvio.htm.

[30] C. Schonenberger et al. -. *J. Phys. Chem.*, 99:3259–3271, 1995.

[31] Y. Katayama et al. Cyclic amp detection by electrode modified with 17mer oligopeptide. *Chem. Lett.*, page 884, 1997.

[32] Molecular Probes Inc: http://www.probes.com.

[33] Internal notes by Paul Hansma.

[34] P. Horowitz and Winfield Hill. *The Art of Electronics*. Cambridge University Press, 2001.